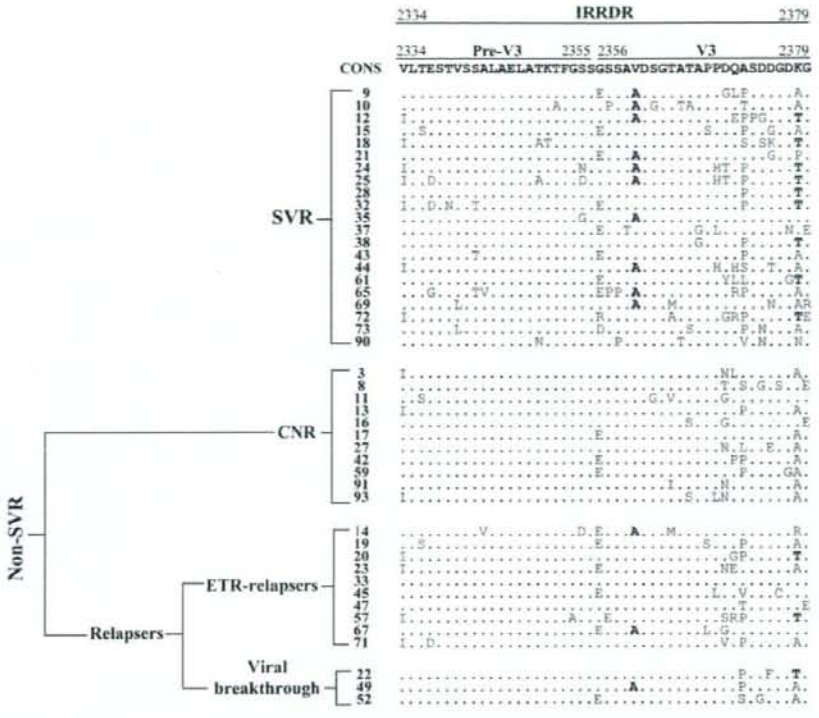

Fig. 2. Sequence alignment of IRRDR (Pre-V3 plus V3 regions) of NS5A of HCV-1b obtained from the pretreatment sera. The consensus sequence (Cons) is shown on the top. The Cons sequence differs from a prototype sequence of IFN-resistant HCV-1b (HCV-J; DDBJ/EMBL/GenBank accession no. D90208) by a single residue at position 2367 (alanine instead of glycine). The numbers along the sequence indicate aa positions. Dots indicate residues identical to those of the Cons sequence. Ala^{2360} and Thr^{2378} are written in boldface.

more mutations in ISDR (data not shown), the criterion for IFN-sensitive HCV strains according to Enomoto et al.[8,9] Although there appeared to be a trend for patients with HCV having four or more mutations in ISDR toward SVR (3 of 4), the difference was not statistically significant. Also, the prevalence of HCV with four or more mutations in ISDR was not significantly different between SVR (3 of 21; 14.3%) and non-SVR (1 of 24; 4.2%). It would be interesting to note, however, that all three HCV strains with four or more mutations in ISDR obtained from SVR (nos. 10, 65, and 72) had HCV of IRRDR of 6 or greater, whereas the only one strain with four or more mutations in ISDR from non-SVR (no. 13) had three mutations in IRRDR (data not shown). It is thus possible that the IRRDR sequence variation is associated with PEG-IFN/RBV responsiveness more closely than is the ISDR variation.

Table 5. Multivariate Logistic Regression Analysis to Identify Independent SVR Predictors

Factor	Odds (95% CI)	*P* value
Multivariate analysis 1		
IRRDR ≥ 6	16.0 (2.4-104.3)	0.004
Ala^{2360}	7.1 (0.8-66.8)	0.09
Thr^{2378}	4.1 (0.5-30.9)	0.17
Platelets	1.1 (0.9-1.4)	0.27
Multivariate analysis 2		
IRRDR mutations as a continuous variable	1.8 (1.1-3.1)	0.02
Ala^{2360}	9.3 (1.1-78.8)	0.04
Thr^{2378}	4.9 (0.7-33.3)	0.1
Platelets	1.2 (1.0-1.5)	0.08

Only factors that were significantly associated with SVR in univariate analysis were included in multivariate logistic regression analysis.

Abbreviations: IRRDR, interferon/ribavirin resistance-determining region; Ala^{2360}, alanine at position 2360; Thr^{2378}, threonine at position 2378, CI; confidence interval.

Correlation Between Rapid Reduction of HCV Core Antigen Titers and the Sequence Variation in IRRDR of HCV NS5A Obtained from the Pretreated Sera. As stated before, there was no significant difference in the mean values of initial HCV core antigen titers between patients with SVR and those with non-SVR (Table 2). However, we observed a strong association of SVR with rapid reduction of HCV core antigen titers during the very early stages of treatment, that is, 24 hours and 1, 2, and 4 weeks after the initiation of treatment (data not shown). Therefore, we analyzed whether the degree of sequence variation in IRRDR correlated with the very rapid reduction (24 hours after the first dose of PEG-IFN/RBV) of HCV core antigen titers. The result obtained clearly demonstrated a significant correlation between IRRDR of 6 or greater and the very rapid reduction of HCV core antigen titers 24 hours and 1, 2, and 4 weeks

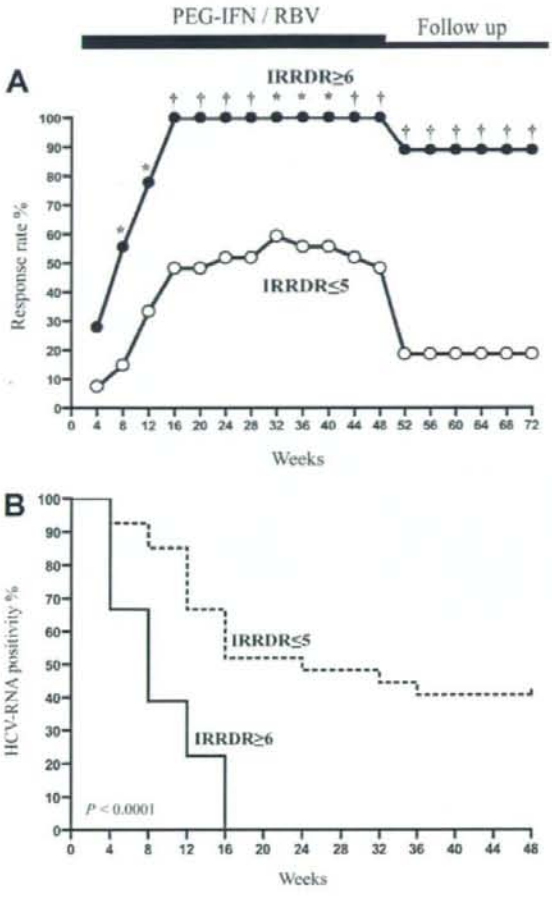

Fig. 3. Time course of HCV clearance during IFN/RBV treatment and follow-up period. (A) The viral clearance rates of patients infected with HCV isolates with six or more mutations in IRRDR (IRRDR ≥ 6) or five or fewer mutations (IRRDR ≤ 5) at 4-week intervals during the whole observation period. *$P < 0.01$; †, $P < 0.001$ (Fisher's exact probability test). (B) Kaplan-Meier HCV survival curve analysis based on serum HCV-RNA positivity during IFN/RBV treatment course (48 weeks) for HCV isolates with IRRDR of 6 or greater and IRRDR of 5 or fewer. $P < 0.0001$ (log-rank test).

after the initiation of treatment (Table 6). Most notably, all 18 patients infected with HCV isolates of IRRDR of 6 or greater achieved significant (≥1 log) reduction or disappearance of serum HCV core antigen titers 24 hours after the first dose of PEG-IFN/RBV.

Proposed Markers for Prediction of Various Virological Responses During PEG-IFN/RBV Combination Therapy. As described, IRRDR of 6 or greater and Ala[2360] were statistically selected as independent SVR predictors. Therefore, we aimed to assess their predictability, in terms of positive and negative predictive values, for various virological responses to PEG-IFN/RBV combination therapy (Table 7). IRRDR greater than or equal to 6 could predict EVR(12w), ETR, and SVR with the positive predictive values of 78% ($P = 0.01$), 100% ($P = 0.000007$), and 89% ($P = 0.0007$), respectively. Moreover, the negative predictive value of IRRDR of 6 or greater for non-SVR was 81% ($P = 0.0008$). Thus, IRRDR of 6 or greater would be useful to predict not only SVR but also non-SVR. Similarly, Ala[2360] could also predict ETR and SVR with positive predictive values of 92% ($P = 0.002$) and 77% ($P = 0.046$), respectively.

Discussion

A substantial proportion of HCV-1b–infected patients do not respond to IFN/RBV combination therapy. Given the significant side effects and high cost associated with this combination therapy, it would be of great utility if clinicians could predict, either before or during the treatment, which patients would, or would not, achieve SVR. Useful predictors of SVR must have a high positive predictive value; conversely, useful predictors of non-SVR must have high negative predictive value.[5] Most recent studies have focused on the possible correlation between the likelihood of achieving SVR and viral clearance kinetics during the first few months of the treatment.[25,26] Conversely, some studies dealt with the possible correlation between SVR and sequence variation within a part of NS5A, especially the V3 region.[12-20]

Table 6. Significant Correlation Between the Rapid Reduction of HCV Core Antigen Titers and IRRDR Sequence Variations

	No. of Patients With Significant Reduction of HCV Core Antigen Titers / No. of Total							
Criteria	24 Hours* (≥ 1 log)†	P Value‡	1 Week* (≥ 1 log)†	P Value‡	2 Weeks* (≥ 1.5 log)†	P Value‡	4 Weeks* (≥ 2 log)†	P Value‡
IRRDR ≥ 6	18/18	<0.0001	15/18	0.002	13/18	0.016	16/18	0.0007
IRRDR ≤ 5	10/27		9/27		9/27		10/27	

*Period after initiation of IFN/RBV therapy.

†Criteria of the significant reduction of HCV core antigen titers. Two (both at 24 hours and 1 week) and three patients (both at 2 and 4 weeks) who achieved disappearance of serum HCV core antigen were also considered to meet these criteria.

‡Fisher's exact test.

Abbreviations: IRRDR, interferon/ribavirin resistance-determining region; IFN/RBV, interferon/ribavirin.

Table 7. Positive Predictive Value, Negative Predictive Value, Sensitivity and Specificity of IRRDR ≥ 6 and Ala^{2360} on the Likelihood of Achieving Various Virological Responses

Virological Response	IRRDR ≥ 6				Ala^{2360}			
	PPV	NPV	Sensitivity	Specificity	PPV	NPV	Sensitivity	Specificity
EVR (12W)	78% (14/18)	67% (18/27)	61% (14/23)	82% (18/22)	69% (9/13)	56% (18/32)	39% (9/23)	82% (18/22)
ETR	100% (18/18)	56% (15/27)	58% (18/31)	100% (14/14)	92% (12/13)	41% (13/32)	39% (12/31)	93% (13/14)
SVR	89% (16/18)	81% (22/27)	76% (16/21)	92% (22/24)	77% (10/13)	66% (21/32)	48% (10/21)	88% (21/24)

Abbreviations: IRRDR, interferon/ribavirin resistance-determining region; Ala^{2360}, alanine at position 2360; EVR, early virological response; ETR, end-of-treatment response; SVR, sustained virological response; PPV, positive predictive value; NPV, negative predictive value.

We previously reported that a high degree of sequence variation (≥6 mutations) in IRRDR was significantly correlated with the EVR by week 16 in HCV-1b–infected patients treated with PEG-IFN/RBV combination therapy.[21] In the current follow-up study, we aimed to investigate whether the IRRDR sequence variation is correlated also with SVR. By using different statistical approaches, the results obtained clearly demonstrated that the high degree of sequence variation in IRRDR (IRRDR ≥6) significantly correlated with SVR, whereas the low degree of sequence variation in this region (IRRDR ≤5) correlated with non-SVR. Nearly two-thirds of patients with SVR had HCV of IRRDR of 6 or greater, whereas only 2 (8%) of 24 patients with non-SVR did ($P < 0.0001$) (Table 4). Notably, 16 of the 18 patients infected with HCV of IRRDR of 6 or greater achieved SVR. Accordingly, the positive predictive value and negative predictive value of IRRDR greater than or equal to 6 for SVR and non-SVR were 89% ($P = 0.0007$) and 81% ($P = 0.0008$), respectively (Table 7). Our current results thus strongly suggest that IRRDR greater than or equal to 6 would be a useful marker for prediction of SVR.

It was reported that the determination of HCV core antigen levels in the serum was an accurate and reliable alternative to monitor HCV RNA titers and that rapid reduction of HCV core antigen levels within a few weeks after the initiation of the therapy could predict treatment outcome in patients receiving PEG-IFN/RBV combination therapy.[27-29] Indeed, we found a strong association between the likelihood of achieving SVR and rapid reduction of HCV core antigen during the first 4 weeks of PEG-IFN/RBV combination therapy. More importantly, we found a significant correlation between the rapid reduction of HCV core antigen titers and the degree of sequence variation in IRRDR. Notably, all the patients infected with HCV of IRRDR greater than or equal to 6 showed a significant (≥1 log) reduction or disappearance of serum HCV core antigen titers 24 hours after the first dose of PEG-IFN/RBV (Table 6). This, in particular, suggests a possible influence of IRRDR of 6 or greater on HCV replication kinetics during IFN-based therapy because the direct effect of IFN begins a few hours after the first dose. Moreover, IRRDR greater than or equal to 6 was significantly associated with rapid clearance of serum HCV RNA as early as week 8 during PEG-IFN/RBV combination therapy (Fig. 3). These results collectively reinforce the possible correlation between the sequence variation in IRRDR and HCV clearance by the IFN-based therapy.

We also examined whether the criterion of IRRDR of 6 or greater was applicable to previously reported studies, for which information on both treatment outcome (responder versus nonresponder) and IRRDR sequences are available.[8,13] As shown in Table 8, the average numbers of amino acid variations from the same consensus sequence used in the current study were significantly larger for SVR than for non-SVR in a study with Japanese patients ($P = 0.003$)[8] and hovered at nearly a significant level in a study with European patients ($P = 0.06$).[13] More importantly, the criterion of IRRDR greater than or equal to 6 could significantly differentiate between responders and nonresponders in the Japanese study ($P = 0.003$) and also hovered at nearly a significant level in the European study ($P = 0.058$). It should be noted that, in the latter study, there were only three patients who had HCV with IRRDR of 6 or greater, all of whom became SVR. Taken together, these results suggest the useful application of IRRDR of 6 or greater as an SVR marker even in different geographical regions, although the prevalence of HCV with IRRDR of 6 or greater may vary with different regions of the world.

Although we observed significant correlation between the overall number of mutations in IRRDR and PEG-IFN/RBV responsiveness, we also found particular amino acid mutations, Ala^{2360} and Thr^{2378}, that were significantly associated with SVR (Table 4 and Fig. 2). In particular, Ala^{2360} was identified as an independent SVR marker. In this connection, it should be noted that four of five HCV isolates of IRRDR of 5 or less obtained from patients with SVR had either Ala^{2360} or Thr^{2378}. Furthermore, 20 (95%) of 21 HCV isolates obtained from pa-

Table 8. Comparative Analysis of the Mean Numbers of aa Mutations in IRRDR in Previously Reported Japanese and European Studies

Study	Factor	SVR	Non-SVR	*P* Value
Enomoto et al.[8]	No. of IRRDR mutations	7.6 ± 2.6*	3.7 ± 2.0	0.003†
	No. of patients with IRRDR ≥ 6	8	1	0.003‡
	IRRDR ≤ 5	1	8	
Duverlie et al.[13]	No. of IRRDR mutations	5.6 ± 2.3	4.2 ± 0.8	0.06†
	No. of patients with IRRDR ≥ 6	3	0	0.056‡
	IRRDR ≤ 5	5	11	
This study	No. of IRRDR mutations	6.1 ± 2.1	3.9 ± 1.4	0.0006†
	No. of patients with IRRDR ≥ 6	16	2	< 0.0001‡
	IRRDR ≤ 5	5	22	

NOTE. Same consensus sequence was used in this comparative analysis.
*Mean ± SD.
†Student *t* test.
‡Fisher's exact test.
Abbreviations: aa, amino acid; IRRDR, interferon/ribavirin resistance-determining region; SVR, sustained virological response.

tients with SVR had either one of the three factors (IRRDR ≥6, Ala^{2360}, or Thr^{2378}). To our knowledge, there is no known CD4 or CD8 epitope(s) in IRRDR so far reported. Interestingly, however, Neumann-Haefelin et al.[30] recently identified an HLA-A26 $CD8^+$ T-cell epitope located at position 2416, 37 aa distant from IRRDR. This epitope was shown to be targeted in all patients with acute resolving HCV infection examined. Further studies are needed to elucidate the role(s) for the distal carboxy terminal region of NS5A, including IRRDR, in both IFN/RBV responsiveness and T cell–mediated virus clearance.

In conclusion, our results suggest that a high degree of sequence variation in IRRDR (IRRDR ≥6), and a particular aa mutation (Ala^{2360}) to a lesser extent, would be a useful marker to predict SVR.

References

1. Hoofnagle JH, Seeff LB. Peginterferon and ribavirin for chronic hepatitis C. N Engl J Med 2006;355:2444-2451.
2. Pawlotsky JM. Therapy of hepatitis C: from empiricism to eradication. HEPATOLOGY 2006;43:S207-S220.
3. Manns MP, McHutchison JG, Gordon SC, Rustgi VK, Shiffman M, Reindollar R, et al. Peginterferon alfa-2b plus ribavirin compared with interferon alfa-2b plus ribavirin for initial treatment of chronic hepatitis C: a randomised trial. Lancet 2001;358:958-965.
4. Fried MW, Shiffman ML, Reddy KR, Smith C, Marinos G, Goncales FL Jr, et al. Peginterferon alfa-2a plus ribavirin for chronic hepatitis C virus infection. N Engl J Med 2002;347:975-982.
5. Ferenci P, Fried MW, Shiffman ML, Smith CI, Marinos G, Goncales FL Jr, et al. Predicting sustained virological responses in chronic hepatitis C patients treated with peginterferon alfa-2a (40 KD)/ribavirin. J Hepatol 2005;43:425-433.
6. Ferenci P. Predictors of response to therapy for chronic hepatitis C. Semin Liver Dis 2004;24(Suppl 2):25-31.
7. Welker MW, Hofmann WP, Welsch C, von Wagner M, Herrmann E, Lengauer T, et al. Correlation of amino acid variations within nonstructural 4B protein with initial viral kinetics during interferon-alpha-based therapy in HCV-1b-infected patients. J Viral Hepatol 2007;14:338-349.
8. Enomoto N, Sakuma I, Asahina Y, Kurosaki M, Murakami T, Yamamoto C, et al. Comparison of full-length sequences of interferon-sensitive and resistant hepatitis C virus 1b: sensitivity to interferon is conferred by amino acid substitutions in the NS5A region. J Clin Invest 1995;96:224-230.
9. Enomoto N, Sakuma I, Asahina Y, Kurosaki M, Murakami T, Yamamoto C, et al. Mutations in the nonstructural protein 5A gene and response to interferon in patients with chronic hepatitis C virus 1b infection. N Engl J Med 1996;334:77-81.
10. Gale MJ Jr, Korth MJ, Tang NM, Tan SL, Hopkins DA, Dever TE, et al. Evidence that hepatitis C virus resistance to interferon is mediated through repression of the PKR protein kinase by the nonstructural 5A protein. Virology 1997;230:217-227.
11. Gale MJ Jr, Korth MJ, Katze MG. Repression of the PKR protein kinase by the hepatitis C virus NS5A protein: a potential mechanism of interferon resistance. Clin Diagn Virol 1998;10:157-162.
12. Nousbaum J, Polyak SJ, Ray SC, Sullivan DG, Larson AM, Carithers RL, Jr, Gretch DR. Prospective characterization of full-length hepatitis C virus NS5A quasispecies during induction and combination antiviral therapy. J Virol 2000;74:9028-9038.
13. Duverlie G, Khorsi H, Castelain S, Jaillon O, Izopet J, Lunel F, et al. Sequence analysis of the NS5A protein of European hepatitis C virus 1b isolates and relation to interferon sensitivity. J Gen Virol 1998;79 (Pt 6):1373-1381.
14. Layden-Almer JE, Kuiken C, Ribeiro RM, Kunstman KJ, Perelson AS, Layden TJ, Wolinsky SM. Hepatitis C virus genotype 1a NS5A pretreatment sequence variation and viral kinetics in African American and white patients. J Infect Dis 2005;192:1078-1087.
15. Vuillermoz I, Khattab E, Sablon E, Ottevaere I, Durantel D, Vieux C, et al. Genetic variability of hepatitis C virus in chronically infected patients with viral breakthrough during interferon-ribavirin therapy. J Med Virol 2004; 74:41-53.
16. Puig-Basagoiti F, Forns X, Furcic I, Ampurdanes S, Gimenez-Barcons M, Franco S, et al. Dynamics of hepatitis C virus NS5A quasispecies during interferon and ribavirin therapy in responder and non-responder patients with genotype 1b chronic hepatitis C. J Gen Virol 2005;86:1067-1075.
17. Sarrazin C, Herrmann E, Bruch K, Zeuzem S. Hepatitis C virus nonstructural 5A protein and interferon resistance: a new model for testing the reliability of mutational analyses. J Virol 2002;76:11079-11090.
18. Murphy MD, Rosen HR, Marousek GI, Chou S. Analysis of sequence configurations of the ISDR, PKR-binding domain, and V3 region as predictors of response to induction interferon-alpha and ribavirin therapy in chronic hepatitis C infection. Dig Dis Sci 2002;47:1195-1205.
19. Veillon P, Payan C, Le Guillou-Guillemette H, Gaudy C, Lunel F. Quasispecies evolution in NS5A region of hepatitis C virus genotype 1b during interferon or combined interferon-ribavirin therapy. World J Gastroenterol 2007;13:1195-1203.

20. Wohnsland A, Hofmann WP, Sarrazin C. Viral determinants of resistance to treatment in patients with hepatitis C. Clin Microbiol Rev 2007;20:23-38.
21. El-Shamy A, Sasayama M, Nagano-Fujii M, Sasase N, Imoto S, Kim SR, et al. Prediction of efficient virological response to pegylated interferon/ribavirin combination therapy by NS5A sequences of hepatitis c virus and anti-NS5A antibodies in pre-treatment sera. Microbiol Immunol 2007;51: 471-482.
22. Okamoto H, Sugiyama Y, Okada S, Kurai K, Akahane Y, Sugai Y, et al. Typing hepatitis C virus by polymerase chain reaction with type-specific primers: application to clinical surveys and tracing infectious sources. J Gen Virol 1992;73(Pt 3):673-679.
23. Lusida MI, Nagano-Fujii M, Nidom CA, Soetjipto, Handajani R, Fujita T, et al. Correlation between mutations in the interferon sensitivity-determining region of NS5A protein and viral load of hepatitis C virus subtypes 1b, 1c, and 2a. J Clin Microbiol 2001;39:3858-3864.
24. Kato N, Hijikata M, Ootsuyama Y, Nakagawa M, Ohkoshi S, Sugimura T, et al. Molecular cloning of the human hepatitis C virus genome from Japanese patients with non-A, non-B hepatitis. Proc Natl Acad Sci U S A 1990;87:9524-9528.
25. Lukasiewicz E, Hellstrand K, Westin J, Ferrari C, Neumann AU, Pawlotsky JM, et al. Predicting treatment outcome following 24 weeks peginterferon alpha-2a/ribavirin therapy in patients infected with HCV genotype 1: utility of HCV-RNA at day 0, day 22, day 29, and week 6. HEPATOLOGY 2007;45:258-259.
26. Jensen DM, Morgan TR, Marcellin P, Pockros PJ, Reddy KR, Hadziyannis SJ, et al. Early identification of HCV genotype 1 patients responding to 24 weeks peginterferon alpha-2a (40 kd)/ribavirin therapy. HEPATOLOGY 2006;43:954-960.
27. Maynard M, Pradat P, Berthillon P, Picchio G, Voirin N, Martinot M, et al. Clinical relevance of total HCV core antigen testing for hepatitis C monitoring and for predicting patients' response to therapy. J Viral Hepat 2003;10:318-323.
28. Bouvier-Alias M, Patel K, Dahari H, Beaucourt S, Larderie P, Blatt L, et al. Clinical utility of total HCV core antigen quantification: a new indirect marker of HCV replication. HEPATOLOGY 2002;36:211-218.
29. Veillon P, Payan C, Picchio G, Maniez-Montreuil M, Guntz P, Lunel F. Comparative evaluation of the total hepatitis C virus core antigen, branched-DNA, and amplicor monitor assays in determining viremia for patients with chronic hepatitis C during interferon plus ribavirin combination therapy. J Clin Microbiol 2003;41:3212-3220.
30. Neumann-Haefelin C, Killinger T, Timm J, Southwood S, McKinney D, Blum HE, et al. Absence of viral escape within a frequently recognized HLA-A26-restricted CD8+ T-cell epitope targeting the functionally constrained hepatitis C virus NS5A/5B cleavage site. J Gen Virol 2007;88: 1986-1991.

Prior Immunization with Severe Acute Respiratory Syndrome (SARS)-Associated Coronavirus (SARS-CoV) Nucleocapsid Protein Causes Severe Pneumonia in Mice Infected with SARS-CoV[1]

Fumihiko Yasui,* Chieko Kai,[‡] Masahiro Kitabatake,[2]* Shingo Inoue,[‖] Misako Yoneda,[‡] Shoji Yokochi,*[§] Ryoichi Kase,* Satoshi Sekiguchi,* Kouichi Morita,[‡] Tsunekazu Hishima,[¶] Hidenori Suzuki,[†] Katsuo Karamatsu,[#] Yasuhiro Yasutomi,[#] Hisatoshi Shida,[**] Minoru Kidokoro,[††] Kyosuke Mizuno,[‡‡] Kouji Matsushima,[§] and Michinori Kohara[3]*

The details of the mechanism by which severe acute respiratory syndrome-associated coronavirus (SARS-CoV) causes severe pneumonia are unclear. We investigated the immune responses and pathologies of SARS-CoV-infected BALB/c mice that were immunized intradermally with recombinant vaccinia virus (VV) that expressed either the SARS-CoV spike (S) protein (LC16m8rVV-S) or simultaneously all the structural proteins, including the nucleocapsid (N), membrane (M), envelope (E), and S proteins (LC16m8rVV-NMES) 7–8 wk before intranasal SARS-CoV infection. The LC16m8rVV-NMES-immunized group exhibited as severe pneumonia as the control groups, although LC16m8rVV-NMES significantly decreased the pulmonary SARS-CoV titer to the same extent as LC16m8rVV-S. To identify the cause of the exacerbated pneumonia, BALB/c mice were immunized with recombinant VV that expressed the individual structural proteins of SARS-CoV (LC16mOrVV-N, -M, -E, -S) with or without LC16mOrVV-S (i.e., LC16mOrVV-N, LC16mOrVV-M, LC16mOrVV-E, or LC16mOrVV-S alone or LC16mOrVV-N + LC16mOrVV-S, LC16mOrVV-M + LC16mOrVV-S, or LC16mOrVV-E + LC16mOrVV-S), and infected with SARS-CoV more than 4 wk later. Both LC16mOrVV-N-immunized mice and LC16mOrVV-N + LC16mOrVV-S-immunized mice exhibited severe pneumonia. Furthermore, LC16mOrVV-N-immunized mice upon infection exhibited significant up-regulation of both Th1 (IFN-γ, IL-2) and Th2 (IL-4, IL-5) cytokines and down-regulation of anti-inflammatory cytokines (IL-10, TGF-β), resulting in robust infiltration of neutrophils, eosinophils, and lymphocytes into the lung, as well as thickening of the alveolar epithelium. These results suggest that an excessive host immune response against the nucleocapsid protein of SARS-CoV is involved in severe pneumonia caused by SARS-CoV infection. These findings increase our understanding of the pathogenesis of SARS. ***The Journal of Immunology*, 2008, 181: 6337–6348.**

From November 2002 to July 2003, an outbreak of severe acute respiratory syndrome (SARS),[4] which originated in China, spread worldwide, resulting in 8098 cases with 774 deaths (http://www.who.int/csr/sars/country/en/index.html). Patients with SARS usually develop high fever followed by severe clinical symptoms, which include acute respiratory distress syndrome with diffuse alveolar damage, and ultimately death. A novel type of coronavirus (CoV), termed SARS-associated CoV (SARS-CoV), was identified as the etiologic agent of SARS (1–3). The genome of SARS-CoV is a single strand of positive-sense RNA of ~30 kb in length with 14 putative open reading frames, which encode nonstructural replicase polyproteins and several structural proteins, including spike (S), envelope (E), membrane (M), and nucleocapsid (N) proteins (4). The S protein of SARS-CoV, like the S proteins of other CoVs, plays an important role in the first step of viral infection by binding to a host cell receptor. Angiotensin-converting enzyme 2 was identified as the host receptor for SARS-CoV (5). Angiotensin-converting enzyme 2 is abundantly expressed in the epithelia of the lung and small intestine and may mediate SARS-CoV entry in humans (6). Although intensive investigations rapidly unraveled the sequence of the SARS-CoV genome and its receptor in humans, the precise molecular mechanism underlying the development of SARS is not fully understood.

The possible roles of host anti-SARS-CoV immune responses have been suggested in severe clinical cases. The uncontrolled release of immune mediators, called a "cytokine storm," has been

*Department of Microbiology and Cell Biology, [†]Laboratory of Electron Microscopy, The Tokyo Metropolitan Institute of Medical Science, [‡]Laboratory Animal Research Center, The Institute of Medical Science, [§]Department of Molecular Preventive Medicine, School of Medicine, The University of Tokyo, and [¶]Department of Pathology, Tokyo Metropolitan Komagome Hospital, Tokyo, Japan; [‖]Department of Virology, Institute of Tropical Medicine, Nagasaki University, Nagasaki, Japan; [#]Laboratory of Immunoregulation and Vaccine Research, Tsukuba Primate Research Center, National Institute of Biomedical Innovation, Ibaraki, Japan; [**]Division of Molecular Virology, Institute for Genetic Medicine, Hokkaido University, Sapporo, Japan; [††]Third Department of Virology, National Institute of Infectious Diseases, Musashimurayama, Japan; and [‡‡]The Chemo-Sero-Therapeutic Research Institute, Kumamoto, Japan

Received for publication January 23, 2008. Accepted for publication August 23, 2008.

The costs of publication of this article were defrayed in part by the payment of page charges. This article must therefore be hereby marked *advertisement* in accordance with 18 U.S.C. Section 1734 solely to indicate this fact.

[1] This study was supported in part by a Grant for Research on Emerging and Re-emerging Infectious Diseases from the Ministry of Health, Labor and Welfare, Japan, by the 21st Century Centers of Excellence program on Global Strategies for Control of Tropical and Emerging Infectious Diseases at Nagasaki University, and by the Ministry of Education, Culture, Sports, Science and Technology of Japan. Strategic cooperation to control emerging and re-emerging infections is funded by the Special Co-ordination Fund for Promoting Science and Technology of the Ministry of Education, Culture, Sports, Science and Technology.

[2] Current address: Department of Immunology, Graduate School of Medicine, Kumamoto University, 1-1-1 Honjo, Kumamoto, 860-8556, Japan.

[3] Address correspondence and reprint requests to Dr. Michinori Kohara, Department of Microbiology and Cell Biology, The Tokyo Metropolitan Institute of Medical Science, 3-18-22 Honkomagome, Bunkyo-ku, Tokyo 113-8613, Japan. E-mail address: kohara-mc@igakuken.or.jp

[4] Abbreviations used in this paper: SARS, severe acute respiratory syndrome; CoV, coronavirus; VV, vaccinia virus; HA, hemagglutinin; MOI, multiplicity of infection; VLP, virus-like particle; $TCID_{50}$, tissue culture ID_{50}.

implicated in the pathogenesis of SARS. However, the cytokine profiles of SARS patient sera do not correlate with the severity of pneumonia because of their diversity. For example, Jones et al. (7) have reported a decreased number of IL-2-, IL-4-, IL-10-, and IL-12-producing cells in SARS-CoV-infected patients. In contrast, Wong et al. (8) have demonstrated increased production of IFN-γ, IL-1, IL-6, and IL-12 p70, but not of IL-2, IL-4, IL-10 or TNF-α, which is consistent with a Th1 response. The data from these adult patients with SARS show no clear trend toward either a Th1 or Th2 bias. These results might be related to patient anamnesis. Therefore, the development of animal models for SARS is needed to understand the pathogenesis of SARS. Non-human primates, mice, ferrets, and hamsters have been found to support the replication of SARS-CoV (9–14). However, an animal model that mimics the clinical symptoms and pathology observed in SARS patients has not been reported to date. Recently, Roberts et al. (15) reported that aged BALB/c mice (older than 12 mo) exhibited high and prolonged levels of viral replication, signs of clinical symptoms, and histopathologic changes in the lung. Aged BALB/c mice represent a conventional animal model that mimics the findings in elderly SARS patients, many of whom exhibit severe disease requiring intensive care and ventilation support, as well as increased mortality.

In the present study, we investigated the pulmonary immune responses and pathologies of intranasally SARS-CoV-infected BALB/c mice older than 6 mo of age that were previously immunized with SARS-CoV structural proteins using vaccinia virus (VV) vectors, by measuring various cytokine mRNAs and histopathologies of the lungs.

Materials and Methods

Cells and viruses

RK13 cells (CCL-37) from the American Type Culture Collection (ATCC) and Vero E6 cells (CRL-1586) from ATCC were cultured in MEM (Nissui Pharmaceutical) that contained 5% FCS. To generate recombinant VV LC16m8, which expresses the structural proteins of SARS-CoV, primary rabbit kidney cell cultures were prepared by overnight digestion with 100 PU/ml dispase (Sanko Jun-yaku) of kidneys extirpated from 7-day-old inbred JW rabbits (Kitayama Labs). The cells were grown in T175 flasks in lactalbumin medium with Hank's salts (LH) that contained 5% FCS, 100 U/ml penicillin, and 100 μg/ml streptomycin. When the cell confluency was ~50%, the culture medium was replaced with lactalbumin medium with Eagle's salts (LE) that contained 5% FCS, 100 U/ml penicillin, and 100 μg/ml streptomycin. SARS-CoV Vietnam/NB-04/2003 strain, which was isolated from the throat wash fluid of one patient (16), was provided by Dr. M. Quynh Le. VVs LC16m8 (m8) and LC16mO (mO) were provided by the Chemo-Sero-Therapeutic Research Institute (Kumamoto, Japan). All work using SARS-CoV was performed in BioSafety Level 3 facilities by personnel wearing powered air-purifying respirators (Shigematsu Works).

Generation of recombinant VV

To generate a pBR322-based plasmid vector (pBMSF) for homologous recombination into the hemagglutinin (HA) locus of m8, we cloned the HA gene, which contained the ATI/p7.5 synthetic hybrid promoter, from the pSFJ1–10 plasmid and inserted it into the pBM vector, which was reconstructed in our laboratory. Full-length cDNAs for the SARS-CoV nucleocapsid (N), membrane (M), and envelope (E) proteins were cloned from the Vietnam/NB-04/2003 strain of SARS-CoV by RT-PCR (16). Full-length SARS-CoV spike (S) protein gene was prepared from pSFJ1-10-SARS-S, which is described in our previous report (17). Next, the genes that encode the SARS-CoV structural proteins were ligated by inserting internal ribosomal entry site sequence of hepatitis C virus (genotypes 2a and 1b/2b) fused with the 2A sequence of foot and mouth disease virus and *Thosea asigna* virus or encephalomyocarditis virus by PCR (see Fig. 1*A*). The generated DNA fragment was digested with *Eco*RI and inserted downstream of the ATI/p7.5 hybrid promoter of pBR322-based plasmid vector pBMSF, thereby generating pBMSF-SARS-NMES. The pBMSF-SARS-NMES plasmid was linearized with *Pvu*I, and transfected into primary rabbit kidney cells that had been infected with m8 at a multiplicity of infection (MOI) of 10. After 36 h, the virus-cell mixture were harvested by scraping, and frozen at −80°C until use. The resulting HA-negative recombinant viruses were purified as previously described (17), and named m8rVV-NMES. Furthermore, recombinant mO that expressed the SARS-CoV N, M, or E protein with a six histidine tag at the C terminus was generated (mOrVV-NHis, mOrVV-MHis, and mOrVV-EHis), as was mO that expressed six histidine-tagged S protein (mOrVV-SHis), as previously described (17).

Western blot analysis

Vero E6 cells were infected with m8rVV-NMES at an MOI of 5. After 18 h, the cells were lysed with lysis buffer (10 mM Tris (pH 7.4), 150 mM NaCl, 1% SDS, 0.5% Nonidet P-40, protease inhibitor cocktail). The cell lysates (30 μg) were resolved by SDS-PAGE and transferred to a polyvinylidene difluoride membrane (Immobilon-P; Millipore). After blocking the membranes with 5% skim milk solution at room temperature for 1 h, the membrane was incubated with polyclonal Abs against the N, M, E, or S protein. Vero E6 cell lysates infected with mOrVV-NHis, mOrVV-MHis, mOrVV-EHis, or mOrVV-SHis was used as positive controls. We used the anti-S polyclonal Abs described in our previous study (17). Polyclonal Abs against N and E proteins were prepared from rabbit sera immunized with KLH-conjugated N peptide (residues aa 250–263) and E peptide (residues aa 61–73). Polyclonal Abs against the M protein were provided by Dr. Mizutani (National Institute of Infectious Diseases, Musashimurayama, Tokyo). We purified the IgG fractions of these antisera using the protein A Ampure PA kit (Amersham Biosciences). After washing with TBS that contained 0.1% Tween 20 (TBST), the membranes were reacted with HRP-conjugated $F(ab')_2$ of anti-rabbit IgG (GE Healthcare). Each specific protein band was visualized using the ECL system (GE Healthcare).

Indirect immunofluorescence analysis

Vero E6 cells were infected with m8rVV-NMES at an MOI of 5 at 30°C for 4 h. The cells were washed with PBS and fixed with cold acetone/methanol (1/1) mixture for 10 min. After blocking with TNB blocking buffer (NEN Life Science Products) at room temperature for 1 h, the fixed cells were incubated with polyclonal Abs against the N, M, or E protein or mAb against the S protein (designated as anti-S-His protein, clone no. 13B8), which was originally prepared in our laboratory, at 4°C overnight. After washing, the cells were incubated with Alexa Fluor 488-conjugated anti-rabbit IgG or mouse IgG Ab at room temperature for 1 h. Nuclei were stained with DAPI (4′,6-diamidino-2-phenylindole). Fluorescence images were acquired using a confocal microscope (LSM510 META; Carl Zeiss).

Confirmation of SARS-CoV-like particle formation

RK13 cells were cultured in 150-mm dishes, and then infected with m8rVV-NMES at an MOI of 5. After 48 h of incubation, the culture supernatants were collected and centrifuged to remove cell debris at 3000 rpm for 30 min at 4°C. The supernatants were concentrated ~100-fold using the Pellicon XL (cut off molecular weight 3×10^5; Millipore). The isolation of virus-like particles (VLP) was performed as previously described, with a slight modification (18). Briefly, the concentrated supernatant was placed on 60% (w/w) sucrose cushion and centrifuged at 4.0×10^4 rpm for 5 h. The opalescent band was collected and centrifuged in a 20–60% (w/w) sucrose gradient at 2.7×10^4 rpm for 4 h, and then divided into 20 fractions. The protein content of each fraction was determined with the DC protein assay kit (Bio-Rad). The 20 μl of each fraction were separated by SDS-PAGE (7.5%, 10%, or 15% polyacrylamide gel), and transferred onto a polyvinylidene difluoride membrane. The membrane was incubated with mAb against S protein (13B8), mAb against N protein (IMG-654; Imgenex) or polyclonal Abs against the M or E protein. After washing, the membranes were reacted and visualized as described. The VLPs in the concentrated culture supernatant were visualized using transmission electron microscopy. For immunogold staining, VLPs were loaded onto a collodion-coated electron microscopy grid for 5 min. After the removal of excess sample solution, polyclonal Ab against S protein was added onto the grid and incubated at room temperature for 1 h. The grids were washed six times with Sorensen's phosphate buffer at room temperature and incubated with 5-nm gold-conjugated anti-rabbit IgG for 1 h. After washing with Sorensen's phosphate buffer for 10 s, the samples were stained with 2% phosphotungstic acid for 1 min. After draining off the excess phosphotungstic acid, the samples were observed under the electron microscopy.

Immunization of rabbits with m8rVV-NMES

Groups of three New Zealand White rabbits (SLC) were immunized intradermally with 1×10^8 PFU/body of m8rVV-NMES or with 1×10^8 PFU/body of m8, at 0 and 6 wk. Sera were collected at the indicated time

points (see Fig. 2A), and used in ELISA analysis and in the in vitro neutralization assay described below. All animal experiments using rabbits were approved by The Tokyo Metropolitan Institute of Medical Science Animal Experiment Committee and were performed in accordance with the animal experimentation guidelines of The Tokyo Metropolitan Institute of Medical Science.

ELISA

Recombinant SARS-CoV N, M, E, and S proteins tagged with six histidines at the C terminus were expressed in RK13 cells by infecting with mOrVV-N-His, mOrVV-E-His, mOrVV-M-His, or mOrVV-S-His at an MOI of 5. These proteins were purified using nickel Sepharose (6 Fast Flow; GE Healthcare). His-tagged E and M proteins were further purified by SDS-PAGE. These full-length structural proteins (0.2 μg/ml, 50 μl/well) were coated onto 96-well plates at 4°C overnight. The plates were blocked with 1% BSA in PBS(−) that contained 0.5% Tween 20 and 2.5 mM EDTA, and then incubated with serial 2-fold dilutions of sera from the rabbits immunized with m8rVV-NMES or m8. After extensive washing, the plates were assayed as previously described, except that *o*-phenylenediamine was used as the substrate (17). The individual SARS-CoV structural protein-specific IgG titers are presented as the end point dilution Ab titers. The end point titer was defined as the reciprocal of the highest dilution of serum at which the absorbance at 490 nm (A_{490}) ratio (A_{490} of m8rVV-NMES-immunized serum/A_{490} of m8-immunized serum (negative control)) was greater than 2.0, as previously described (19).

In vitro neutralization assay for SARS-CoV

The neutralizing Ab titers of the sera of rabbits immunized with m8rVV-NMES or m8 were determined as previously described (17). Briefly, serial 2-fold dilutions of heat-inactivated sera were mixed with equal volumes of 200 tissue culture ID_{50} ($TCID_{50}$) of SARS-CoV and incubated at 37°C for 1 h. Vero E6 cells were then infected with 100 μl of the virus-serum mixtures in 96-well plates. After 5 days (or 6 days in the SARS-CoV challenge experiment) of infection, the neutralization titer was determined as the end point dilution of the serum at which there was 50% inhibition of the SARS-CoV-induced cytopathic effect. The method used for end point calculation was that described by Reed and Muench (20).

SARS-CoV challenge experiment

Female BALB/c mice older than the 6 mo of age (SLC) were used in this study. Four groups of eight BALB/c mice (seven mice in the vehicle-immunized group) were inoculated intradermally with either 1×10^7 PFU/body of m8, m8rVV-S, or m8rVV-NMES or 70 μl of vehicle (MEM without FCS). At 7–8 wk postimmunization, the mice were infected intranasally with 1×10^5 $TCID_{50}$/body of SARS-CoV (20 μl/mouse), as previously described (11). Four mice from each group were sacrificed 2 and 9 days later, except for the three mice of the vehicle-immunized group, which were sacrificed 2 days later. The mice were sacrificed under anesthesia and the lung, liver, small intestine, and spleen were extirpated. Aliquots of these tissues were frozen immediately at −80°C or fixed with 10% formalin. The collected blood was used for the in vitro neutralization assay. In addition, BALB/c mice were injected intradermally with 1×10^7 PFU/body of recombinant VV that expressed each structural protein of SARS-CoV (mOrVV-NHis, mOrVV-MHis, mOrVV-EHis, mOrVV-SHis) with or without LC16mOrVV-SHis (i.e., LC16mOrVV-N, -M, -E, -S alone or LC16mOrVV-N + LC16mOrVV-S, -M + LC16mOrVV-S, or -E + LC16mOrVV-S), and infected with 1×10^5 $TCID_{50}$/body of SARS-CoV more than 4 wk later. After 2 and 9 days, mice ($n = 3$–5 per group) were sacrificed following blood collection under anesthesia, and their lungs were extirpated. All animal experiments using mice were approved by the Animal Experiment Committee at The Institute of Medical Science, University of Tokyo, and were performed in accordance with the animal experimentation guidelines of The Institute of Medical Science, University of Tokyo.

Determination of viral titers in the organs

The SARS-CoV titers in the mouse organs were determined as previously described (11). Briefly, tissue samples (i.e., lung, liver, small intestine, and spleen) were homogenized in a 10-fold volume of Leibovitz 15 medium (Invitrogen). The homogenates were centrifuged at 2000 rpm for 10 min at 4°C. Serial 10-fold dilutions of the supernatants of these homogenates were added to Vero E6 cells seeded on 96-well plates. After 6 days of incubation, the cells were fixed with 10% formalin. Viral titer was determined as the 50% end point dilution of the homogenate that induced the cytopathic effect. The method used for end point calculation was that described by Reed and Muench (20).

Lung histopathology and inflammation scores

In accordance with a previous report (11), 10% formalin-fixed lung tissues of the SARS-CoV-infected mice were embedded in paraffin. Paraffin block sections (4-μm thickness) were stained with H&E staining. The peribronchial and perivascular scores were recorded in a blinded fashion by a pathologist. We evaluated pulmonary pathology using the histopathologic scoring systems developed by Cimolai et al. (21), in which the scoring system is weighted heavily for bronchial lesions. This scoring system allowed us to differentiate the severity of pulmonary pathology in small groups of animals. The pathology grading system consisted of a numerical score ranging from 0 to 26. In brief, each section was scored based upon a cumulative total from five categories that incorporated evaluations of the following: A) number of bronchiolar and bronchial sites affected by the periluminal infiltrate (range, 0 to 3); B) severity of the periluminal infiltrate (range, 0 to 3); C) luminal exudate severity (range, 0 to 2); D) frequency of perivascular infiltrate (range, 0 to 3); and E) severity of parenchymal pneumonia (range, 0 to 5). The accumulated numeric score was derived from the sum of the subscores: A+3(B+C)+D+E. Eosinophils were detected in tissue sections by method of Luna (22).

Extraction of total RNA and quantitative RT-PCR of cytokine or chemokine mRNA

To measure the levels of cytokine or chemokine mRNA, total RNA samples were extracted from the lungs using the RNeasy Mini kit (Qiagen). Quantitative RT-PCR was conducted with TaqMan Gene Expression assays (Applied Biosystems) using the ABI Prism 7700 and Sequence Detection System software v.1.7. The fold change in copy number of each cytokine/chemokine mRNA was revealed using the $2^{-\Delta\Delta C_T}$ method using 18 S rRNA as an endogenous calibrator.

Statistical analysis

Data are presented as mean ± SD. Statistical analysis was performed by one-way ANOVA, followed by the Dunnett or Bonferroni test. A value of $p < 0.05$ was considered to be statistically significant.

Results

Generation of recombinant VV that expresses the structural proteins of SARS-CoV

A multicistronic transgene that expresses simultaneously four structural proteins (N, M, E, and S proteins) of SARS-CoV was constructed and inserted into the HA locus of LC16m8 (m8) by homologous recombination (Fig. 1A). Expression of the transgene was placed under the control of the powerful ATI/p7.5 hybrid promoter. We screened for m8rVV-NMES using the erythrocyte agglutination assay (17), and confirmed the insertion of the transgene by PCR. Expression of the N, M, E, and S proteins in Vero E6 cells infected with m8rVV-NMES was detected by Western blot analysis. Recombinant LC16mO (mO) expressing the C-terminal histidine-tagged N, M, E or S protein (mOrVV-NHis, -MHis, -EHis, and -SHis) was generated as previously described, and used as a positive control for each protein. We also used m8rVV-S (17). As shown in Fig. 1B, the expression levels of the N and S proteins in the m8rVV-NMES-infected cells were high and moderate, respectively. In contrast, the expression levels of the M and E proteins in m8rVV-NMES-infected cells were weaker than those in mOrVV-MHis- and mOrVV-EHis-infected cells. The M protein in the m8rVV-NMES-infected cells was 20 kDa, whereas that in the mOrVV-MHis-infected cells was observed as forms of ~20 kDa (nonglycosylated form) and 25 kDa (glycosylated form) (23). Furthermore, we investigated the cellular localizations of these structural proteins by indirect immunofluorescence (Fig. 1C). In m8rVV-NMES-infected cells, all of the SARS-CoV proteins were localized in the perinuclear regions. In particular, the localization of the N protein in m8rVV-NMES-infected cells was different from that in mOrVV-NHis-infected cells, in which the N-His protein was found diffusely in the cytoplasm. VLPs are formed by the assembly of structural proteins in the cytoplasm, followed by release into the culture medium. By infecting m8rVV-NMES into RK13 cells, we confirmed

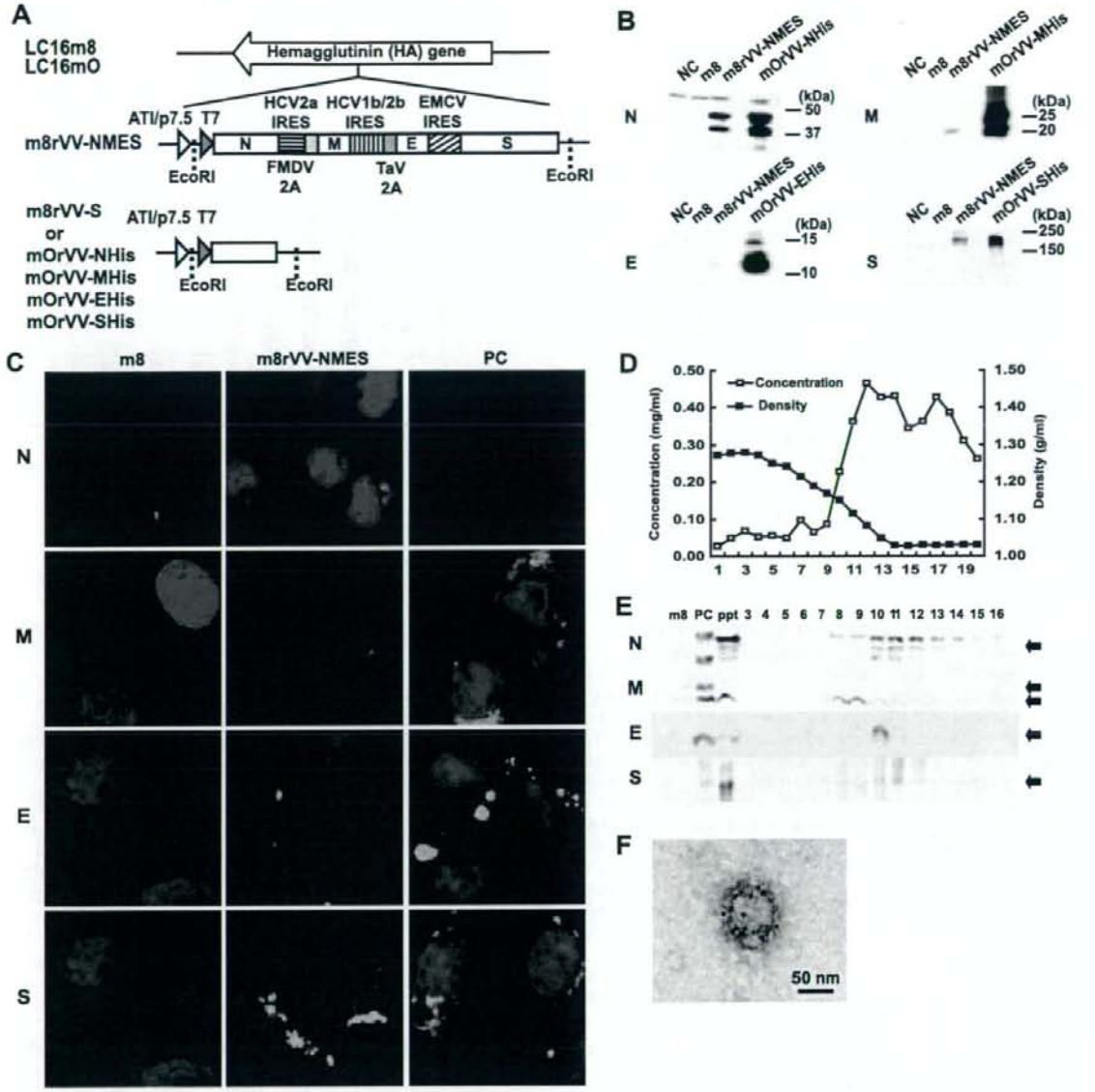

FIGURE 1. Construction of recombinant VV that express four structural proteins of SARS-CoV (m8rVV-NMES). *A*, DNA fragments that encode the SARS-CoV N, M, E, and S proteins were ligated with the internal ribosomal entry site sequence of hepatitis C virus (2a and 1b/2b) and fused with the 2A sequences of foot and mouth disease virus (FMDV) and *Thosea asigna* virus (TaV) or encephalomyocarditis (EMCV). After digestion with *Eco*RI, the DNA fragment was inserted into the pBMSF vector, and the resultant plasmid was designated as pBMSF-NMES. *Pvu*I-linearized pBMSF-NMES was used for homologous recombination into the HA locus of the LC16m8 genome. Recombinant mO that expressed the SARS-CoV N, M, E, or S protein was generated (mOrVV-NHis, -MHis, -EHis, and -SHis) as described in *Materials and Methods*. *B*, Vero E6 cells were infected with m8rVV-NMES or m8. Uninfected Vero E6 cells were used as a negative control (NC). Structural proteins mOrVV-NHis, mOrVV-MHis, mOrVV-EHis, and mOrVV-SHis were used as positive controls. SARS-CoV structural proteins were detected using rabbit polyclonal Abs and donkey anti-rabbit IgG polyclonal Abs, which were conjugated with HRP. The lane between m8rVV-NMES and the mOrVV-N, mOrVV-M, mOrVV-E, and mOrVV-S samples was left empty, to exclude the possibility of leakage of sample solution between lanes. *C*, Vero E6 cells were infected with m8rVV-NMES at an MOI of 5 at 30°C for 4 h. The SARS-CoV proteins in the fixed cells were visualized with the polyclonal Abs against the N, M, or E protein or mAb against the S protein (designated as 13B8). Nuclei were stained with DAPI). Structural proteins mOrVV-NHis, mOrVV-MHis, mOrVV-EHis, and mOrVV-SHis were used as positive controls (PC). *D*, The VLPs were isolated from the culture supernatants of RK13 cells infected with m8rVV-NMES at an MOI of 5 for 48 h at 30°C. After sucrose gradient centrifugation, 20 fractions were collected. *E*, Equal amounts of the gradient fractions (nos. 3–16) were examined by Western blot analyses. m8, m8-infected RK13 cell lysate; ppt, m8rVV-NMES-infected RK13cell lysate; PC, RK13 cell lysates infected with mOrVV-NHis, mOrVV-MHis, mOrVV-EHis, or mOrVV-SHis. *F*, A concentrated culture supernatant was subjected to transmission electron microscopy. VLPs were probed with polyclonal Ab against the S protein and incubated with 5-nm gold-conjugated anti-rabbit IgG.

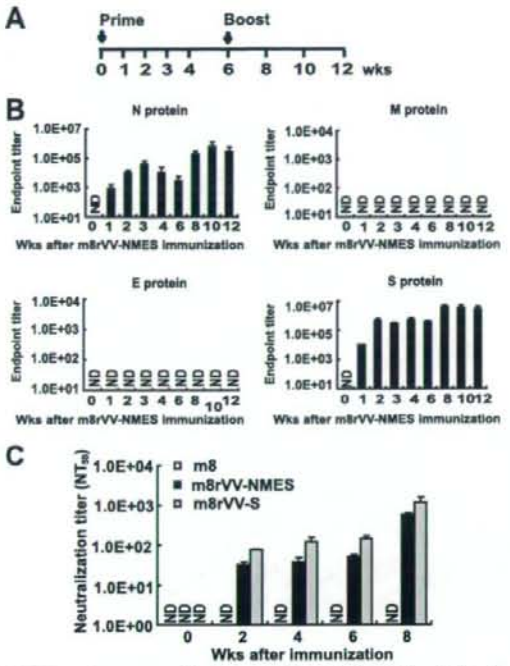

FIGURE 2. Immunogenicity of m8rVV-NMES in rabbits. *A*, New Zealand White rabbits ($n = 3$) were inoculated intradermally with 10^8 PFU/body of m8rVV-NMES or m8 at 0 and 6 wk. Blood samples were collected at the indicated time points. *B*, Induction of serum IgG specific for the four structural proteins of SARS-CoV. The individual SARS-CoV structural protein-specific IgG titers are presented as the end point dilution Ab titers. The end point titer was defined as the reciprocal of the highest dilution of serum at which the absorbance at 490 nm (A_{490}) ratio (A_{490} of m8rVV-NMES-immunized serum/A_{490} of m8-immunized serum (negative control)) was greater than 2.0. *C*, Induction of neutralizing Abs against SARS-CoV. The neutralization titer of m8rVV-NMES-immunized rabbit sera was defined as the end point dilution of the serum at which there was 50% inhibition (NT_{50}) of the SARS-CoV-induced cytopathic effect. Immunization with m8rVVs or m8 was conducted using the schedule described in Fig. 3*A*. ND, Not detectable.

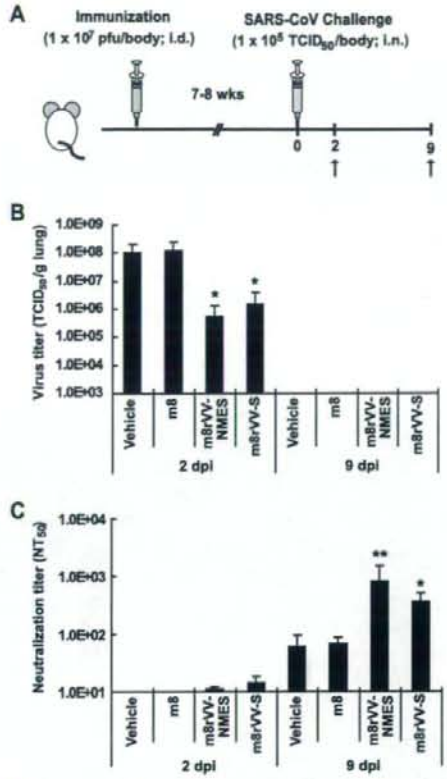

FIGURE 3. SARS-CoV challenge to BALB/c mice immunized with m8rVV-NMES or m8rVV-S. *A*, Four groups of eight BALB/c mice (seven mice in the vehicle-immunized group) were inoculated intradermally with m8rVV-NMES, m8rVV-S, m8, or vehicle and challenged 7–8 wk later with 1×10^5 $TCID_{50}$/body of SARS-CoV delivered via the intranasal route. Blood and lung tissues samples were collected at the indicated time points. *B*, After 2 and 9 days, the titers of SARS-CoV in the lungs of four mice in each group (except for three mice of the vehicle-immunized group, which were examined 2 days later) were determined. Virus titers are expressed as $\log_{10}$ $TCID_{50}$/g of tissue. *C*, At 2 and 9 days after SARS-CoV infection, the serum neutralization titers of all groups were measured as described in *Materials and Methods*. *, $p < 0.05$; **, $p < 0.01$, as compared with both the vehicle- and m8-immunized groups.

the formation of VLPs in the culture medium. After sucrose gradient centrifugation, 20 fractions (500 μl each) were collected (Fig. 1*D*). The four SARS-CoV structural proteins were monitored by Western blot analysis. As shown in Fig. 1*E*, fraction number 10 contained all the SARS-CoV proteins, and the buoyant density of this fraction was ~1.15 g/ml, a value that is consistent with previous reports (18, 24, 25). Moreover, we confirmed the formation of VLPs in the concentrated culture supernatant using scanning electron microscopy and immunogold-labeling with the anti-S protein polyclonal Ab. The particles were 70–100 nm in diameter, which is consistent with the sizes as reported previously (18, 24, 25). The particles were positively stained with immunogold (Fig. 1*F*).

Induction of Abs specific for SARS-CoV structural proteins in rabbits immunized with m8rVV-NMES

To investigate the immunogenicity of m8rVV-NMES, 1×10^8 PFU/body of either m8rVV-NMES or m8, its parental strain, was inoculated intradermally on the backs of New Zealand White rabbits at 0 and 6 wk (Fig. 2*A*). Rabbit antisera specific for the full-length structural proteins of SARS-CoV were detected by ELISA (Fig. 2*B*). In agreement with previous reports (26–28), the N and S proteins both exhibited strong immunogenicity in rabbits. IgG-specific for the N or S protein was induced as early as 1 wk after m8rVV-NMES immunization, and the titer exceeded 1:10000 2 wk later. The titers of Abs against the N and S proteins were dramatically increased by booster immunization with m8rVV-NMES. It was also observed that the Ab titer of the N protein, but not that of the S protein, decreased after reaching the peak titer. Immunization with m8rVV-NMES did not induce Abs specific for the E and M proteins, even after booster immunization (Fig. 2*B*). The antigenicity of the purified E and M proteins coated onto the ELISA plates was confirmed using each rabbit anti-E or anti-M peptide Ab (data not shown). Therefore, we believe that the lack of induction of Abs specific for the E and M proteins in the rabbit sera results from the poor immunogenicity and lower expression levels of these proteins.

Induction of SARS-CoV-neutralizing serum Abs in rabbits by immunizing with m8rVV-NMES

We determined the neutralization titers against SARS-CoV using the same rabbit antisera. The neutralization titer was ~1:30

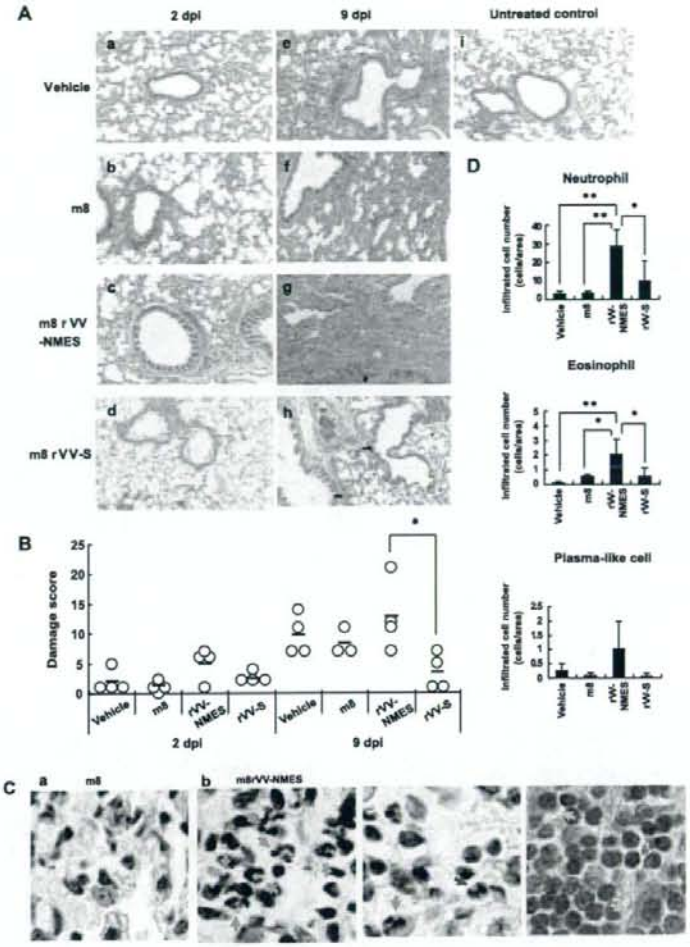

FIGURE 4. Pulmonary histopathology of m8rVV-S-preimmunized BALB/c mice after SARS-CoV challenge. At 7–8 wk after immunization with m8rVV-NMES, m8rVV-S, m8, or vehicle, the mice were infected intranasally with 1×10^5 $TCID_{50}$/body of SARS-CoV. *A*, Four mice from each group (three mice from the vehicle-immunized group were killed 2 days later) were sacrificed 2 and 9 days later. Extirpated lung tissues were fixed with 10% formalin and embedded in paraffin. Paraffin block sections (4-μm thickness) were stained with H&E staining. Histopathologic sections were prepared for vehicle-immunized mice at 2 days postinfection (dpi) (a) and 9 dpi (e), m8-immunized mice at 2 dpi (b) and 9 dpi (f), m8rVV-NMES-immunized mice at 2 dpi (c) and 9 dpi (g), m8rVV-S-immunized mice at 2 dpi (d) and 9 dpi (h), and uninfected mice (i). *B*, The degree of pulmonary inflammation was determined in a blinded fashion on a subjective 27-point scale (0, minimal inflammation; 26, massive inflammation) as described in *Materials and Methods*. Each symbol represents an individual mouse. *, $p < 0.05$. *C*, Representative lung sections from m8-immunized mice (a) and m8rVV-NMES-immunized mice (b) after staining with Luna method (for eosinophils and neutrophils) and H&E (for plasma cells). Arrows indicate neutrophils (yellow), eosinophils (red), and plasma-like cells (green). *D*, The numbers of neutrophils, eosinophils, and plasma-like cells that infiltrated the lung were counted using Luna method and H&E staining. Data are mean ± SD for $n = 5$ mice. Fields viewed at a magnification of ×400. *, $p < 0.05$; **, $p < 0.01$, for significant differences evaluated using the Bonferroni test.

(range, 1:25 to 1:36) after 2 wk, and was sustained for 6 wk (Fig. 2*C*). Booster immunization with m8rVV-NMES further increased the neutralization titer more than 10-fold 2 wk later. These values are somewhat lower than those induced by m8rVV-S in our previous report (17). In contrast, the antisera from rabbits immunized with m8 did not exhibit any neutralizing activity against SARS-CoV (Fig. 2*C*).

SARS-CoV challenge of BALB/c mice having prior immunization with m8rVV-NMES or m8rVV-S

As m8rVV-NMES and m8rVV-S could induce high levels of neutralizing Abs against SARS-CoV (Fig. 2*C*), we investigated the influences of m8rVV-NMES and m8rVV-S on SARS-CoV challenge of BALB/c mice (Fig. 3*A*). The m8rVV-NMES and m8rVV-S constructs were inoculated intradermally on the backs of BALB/c mice at 1×10^7 PFU/body. At 7–8 wk after this single immunization, the mice were infected intranasally with SARS-CoV at 1×10^5 $TCID_{50}$/body. After 2 and 9 days, the lung, liver, small intestine, and spleen were extirpated from the mice under anesthesia, and the SARS-CoV titers were measured. As shown in Fig. 3*B*, 200- and 100-fold reductions in pulmonary virus titers were observed in the m8rVV-NMES-immunized and m8rVV-S-immunized groups 2 days after infection. The virus titers in the lungs of the m8rVV-NMES-immunized and m8rVV-S-immunized groups were 5.40×10^5 and 1.52×10^6 $TCID_{50}$/g of lung, respectively. In contrast, the vehicle-immunized and LC16m8-immunized groups exhibited virus titers of 1.07×10^8 and 1.18×10^8 $TCID_{50}$/g of lung, respectively. The virus was not detected in the lungs of any group 9 days later, as reported previously (11, 15). In contrast, virus titers in other organs, including liver, small intestine, and spleen, were lower than that of the detection limit 2 and 9 days after infection (data not shown).

We also measured the neutralization titers in these mice sera 2 and 9 days after SARS-CoV infection (Fig. 3*C*). Two days postinfection, the neutralization titers of the m8rVV-NMES-immunized and m8rVV-S-immunized groups were 1:11.1 ± 1.01 and 1:14 ± 3.94, respectively, whereas those of the negative control groups were below the limit of detection. At 9 days postinfection, the serum neutralization titers of m8rVV-NMES-immunized and m8rVV-S-immunized groups had increased to 1:838.0 ± 681.0 and 1:367.9 ± 132.1, respectively. In contrast, the serum neutralizing titers of the vehicle-immunized and m8-immunized groups were 1:59.7 ± 35.4 and 1:67.8 ± 18.6, respectively. These results suggest that both the m8rVV-NMES- and m8rVV-S-immunized groups could elicit neutralizing Abs against SARS-CoV and alleviate SARS-CoV infection.

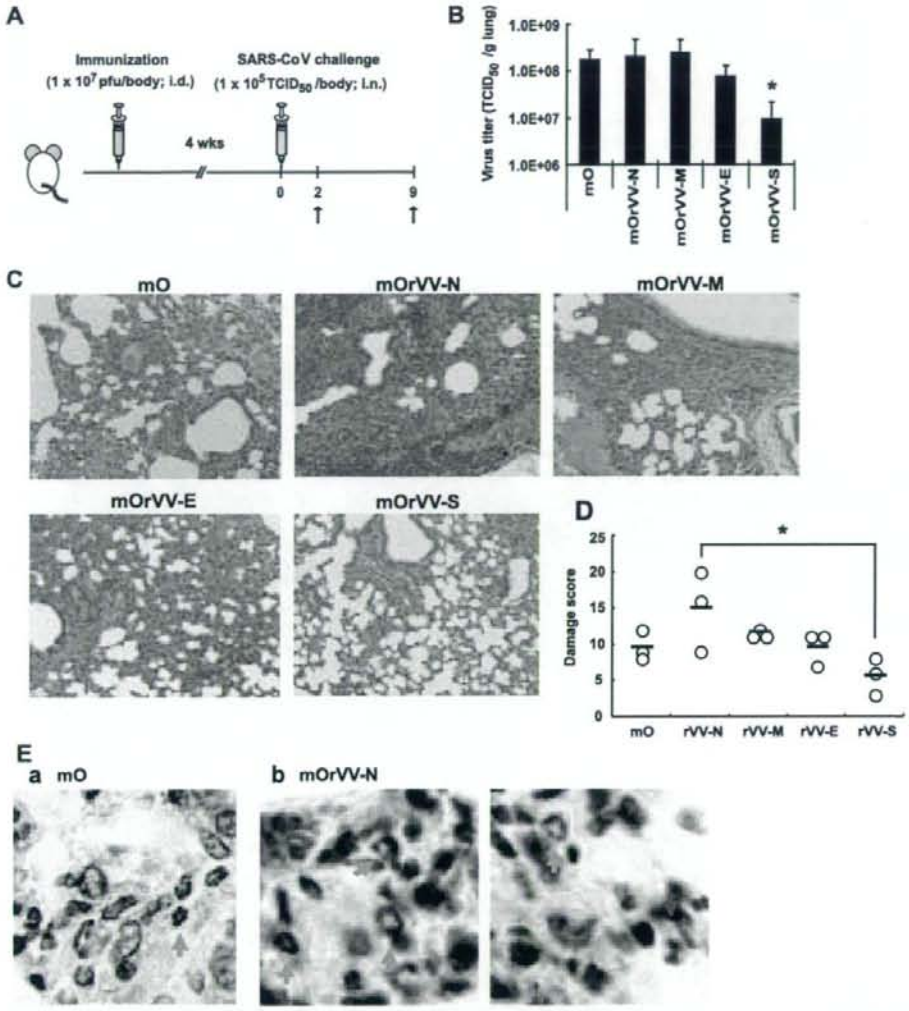

FIGURE 5. Identification of SARS-CoV structural protein implicated in severe pulmonary inflammation. *A*, Five groups of six BALB/c mice were inoculated intradermally with mOrVV-NHis, mOrVV-MHis, mOrVV-EHis, mOrVV-SHis, or mO and challenged 4 wk later with 1×10^5 $TCID_{50}$/body of SARS-CoV via the intranasal route. *B*, After 2 days, the titers of SARS-CoV in the lungs of three mice in each group were determined. Virus titers are expressed as $\log_{10}$ $TCID_{50}$/g of tissue. *, $p < 0.05$, as compared with the mO-immunized group using the Dunnett test. *C*, Histopathologic findings for all the groups 9 days after SARS-CoV infection. Extirpated lung tissues were fixed with 10% formalin and embedded in paraffin. Paraffin block sections (4-μm thickness) were subjected to H&E staining. *D*, The degree of pulmonary inflammation was determined in a blinded fashion on a subjective 27-point scale (0, minimal inflammation; 26, massive inflammation). Each symbol represents an individual mouse. *, $p < 0.05$. *E*, Representative lung sections from mO-immunized mice (a) and mOrVV-N-immunized mice (b) after staining with Luna method (for eosinophils and neutrophils). Arrows indicate neutrophils (yellow) and eosinophils (red).

Histopathologic findings in the lungs of m8rVVs-immunized BALB/c mice after SARS-CoV infection

We performed histopathologic analyses of lung tissues. Two days after SARS-CoV infection, the vehicle-, m8-, and m8rVV-S-immunized groups showed only slight pulmonary inflammation (Fig. 4*A*, a, b, and d), whereas the m8rVV-NMES-immunized group showed infiltration of lymphocytes into the areas surrounding the bronchi and slight thickening of the alveolar epithelium (Fig. 4*A*, c). We scored pulmonary inflammation in all the groups 2 days after SARS-CoV infection as follows (Fig. 4*B*): in the m8rVV-NMES-immunized group, 5.00 ± 2.71; in the vehicle-immunized group, 2.00 ± 2.00; in the m8-immunized group, 1.33 ± 0.82; and in the m8rVV-S-immunized group, 2.50 ± 1.00. At 9 days postinfection, the vehicle-, m8-, and m8rVV-NMES-immunized groups exhibited severe pulmonary inflammation, i.e., infiltration of inflammatory cells and thickening of alveolar epithelia (Fig. 4*A*, e, f, and g). In contrast, the m8rVV-S-immunized group showed only slight pulmonary inflammation (Fig. 4*A*, h). As shown in Fig. 4*B*, the pulmonary inflammation score for the m8rVV-NMES-immunized group (12.75 ± 2.87) 9 days after SARS-CoV infection was significantly higher than that for the m8rVV-S-immunized group (3.50 ± 3.00). In contrast, this score was comparable to those obtained for the vehicle-immunized and m8-immunized groups (9.75 ± 2.87 and

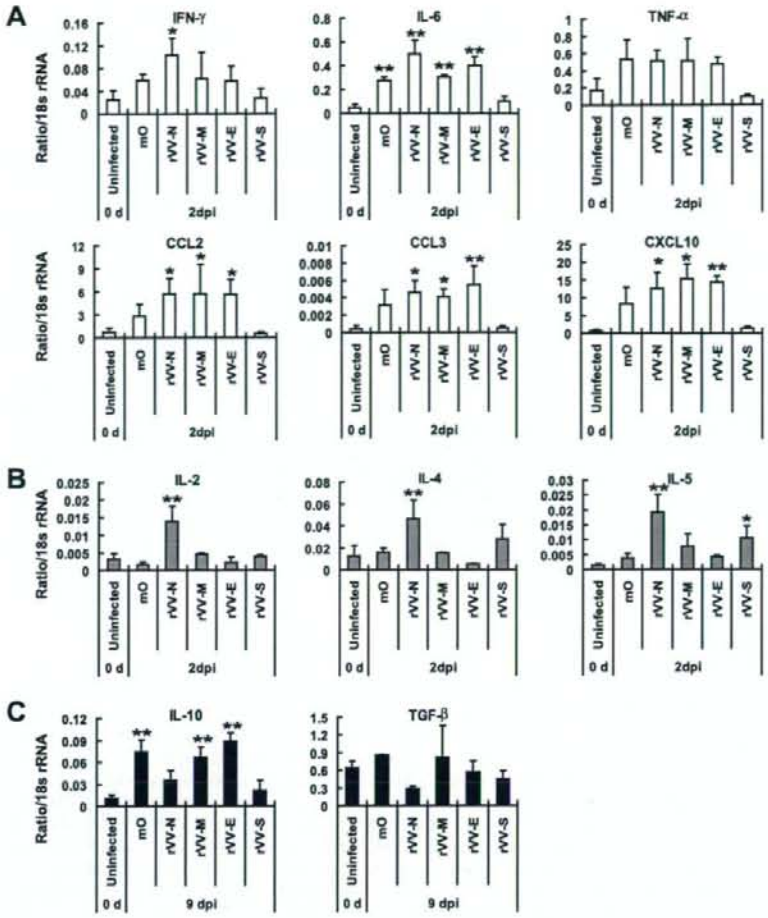

FIGURE 6. Cytokine profiles of the lungs of BALB/c mice preimmunized with each SARS-CoV structural protein and challenged with SARS-CoV. Three mice from each group were sacrificed 2 and 9 days postinfection. The total RNA of the lung was extracted. Quantitative RT-PCR was conducted as described in *Materials and Methods*. The fold change in copy number of each cytokine or chemokine mRNA was calculated by the $2^{-\Delta\Delta Ct}$ method using 18 S rRNA as an endogenous calibrator. *, $p < 0.05$; **, $p < 0.01$, as compared with the uninfected control group using the Bonferroni test. *A*, The levels of mRNA for proinflammatory cytokines and chemokines 2 days after SARS-CoV infection. *B*, The mRNA expression levels of cytokines related to T cell activation 2 days after SARS-CoV infection. *C*, The mRNA expression levels of anti-inflammatory cytokines 9 days after SARS-CoV infection.

8.33 ± 2.31, respectively). The m8rVV-NMES-immunized group exhibited as severe inflammation as the control groups, although m8rVV-NMES contains the S protein and protects as well as m8rVV-S against SARS-CoV infection. In addition, marked infiltration of neutrophils, eosinophils, plasma-like cells, and lymphocytes was observed in the m8rVV-NMES-immunized group, as compared with the control groups, after SARS-CoV infection (Fig. 4*C*, b and *D*).

These results suggest that the severe pulmonary inflammation seen in m8rVV-NMES-immunized mice after SARS-CoV infection results from host immune responses rather than a direct cytopathic effect of SARS-CoV, because the virus titers for all the group were negligible 9 days after SARS-CoV infection and the virus titer of the m8rVV-NMES-immunized group was significantly decreased 2 days postinfection.

Identification of the factor that results in the exacerbation of pulmonary inflammation in m8rVV-NMES-immunized BALB/c mice after SARS-CoV infection

We hypothesized that the severe pulmonary inflammation seen in the m8rVV-NMES-immunized mice resulted from the host immune responses to SARS-CoV components expressed by m8rVV-NMES. This notion was supported by the observation of negligible virus titers 9 days after SARS-CoV infection. Therefore, we investigated the influence of recombinant VV expressing each structural protein of SARS-CoV (mOrVV-NHis, mOrVV-MHis, mOrVV-EHis, and mOrVV-SHis) on subsequent intranasal infection with SARS-CoV. BALB/c mice were immunized with mOrVV-NHis, -MHis, -EHis, and -SHis at 1×10^7 PFU/body, and 4 wk later infected intradermally with 1×10^5 $TCID_{50}$ of SARS-CoV (Fig. 5*A*). After 2 and 9 days, three mice from each group were sacrificed following blood collection under anesthesia, and their lungs were extirpated. Consistent with earlier results, a significant reduction of pulmonary virus titer was observed after 2 days in only the mOrVV-SHis-immunized group (Fig. 5*B*). In contrast, immunization with the other SARS-CoV structural proteins, including the N, M, and E proteins, did not confer protection against the subsequent SARS-CoV infection. As shown in Fig. 5*C*, the alleviation of pulmonary inflammation was also observed in the mOrVV-SHis-immunized group. Severe infiltration of lymphocytes and thickening of the alveolar epithelia were observed in the lung tissues of the mOrVV-NHis-immunized mice 9 days after SARS-CoV infection (Fig. 5*C*). The pulmonary damage in the mOrVV-NHis-immunized mice (15.00 ± 5.56) was significantly more severe than that in the mOrVV-SHis-immunized mice (5.67 ± 2.52) (Fig. 5*D*). However, there were no significant differences among the other groups. Furthermore, infiltration of neutrophils, eosinophils, and lymphocytes was observed in the

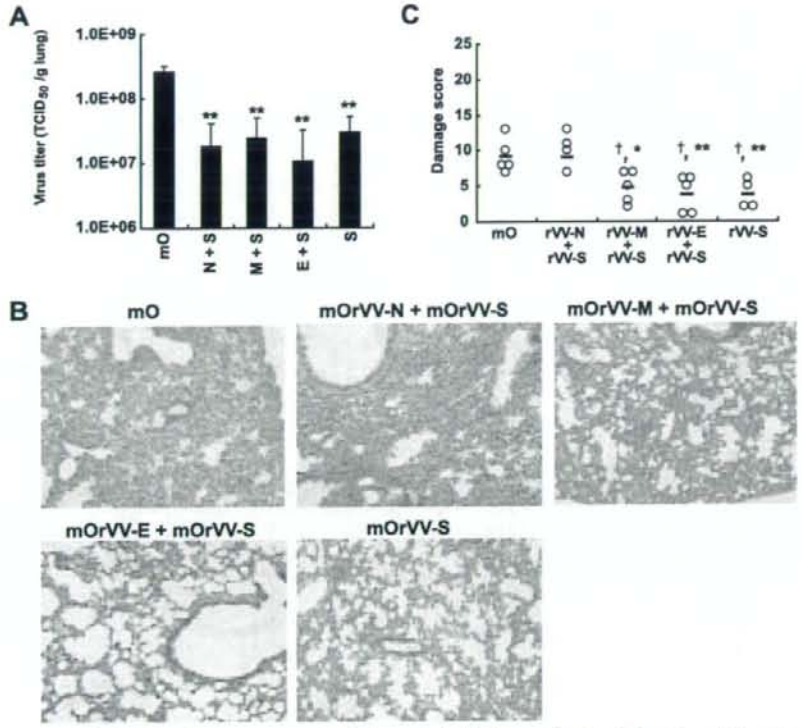

FIGURE 7. Severe pneumonia in BALB/c mice that were previously immunized with the combination of N protein and S protein of SARS-CoV. *A*, Five groups of BALB/c mice ($n = 8–10$ per group) were inoculated intradermally with the combinations of mOrVV-NHis and mOrVV-SHis (mOrVV-N+S), mOrVV-MHis and mOrVV-SHis (mOrVV-M+S), mOrVV-EHis and mOrVV-SHis (mOrVV-E+S), mOrVV-SHis, and mO, and challenged 7 wk later with 1×10^5 $TCID_{50}$/body of SARS-CoV via the intranasal route. After 2 days, the titers of SARS-CoV in the lungs of $n = 3–5$ mice from each group were determined. Virus titers are expressed as $\log_{10}$ $TCID_{50}$/g of tissue. *, $p < 0.05$, **, $p < 0.01$, as compared with the mO-immunized group using the Bonferroni test. *B*, Histopathologic findings for all the groups 9 days after SARS-CoV infection. Extirpated lung tissues were fixed with 10% formalin and embedded in paraffin. Paraffin block sections (4-μm thickness) were subjected to H&E staining. *C*, The degree of pulmonary inflammation was determined in a blinded fashion on a subjective 27-point scale (0, minimal inflammation; 26, massive inflammation). Each symbol represents an individual mouse. †, $p < 0.05$; ‡, $p < 0.01$, as compared with the mO-immunized group using the Bonferroni test. *, $p < 0.05$; **, $p < 0.01$, as compared with the mOrVV-N + S-immunized group using the Bonferroni test.

mOrVV-NHis-immunized mice after SARS-CoV infection (Fig. 5*E*, b), although the extent of infiltration of these cells into the lungs of these mice was somewhat lower than that observed in the m8rVV-NMES-immunized mice after SARS-CoV infection (Fig. 4*D*). This may explain the observed differences in the histopathologic findings for the mOrVV-NHis-immunized mice and m8rVV-NMES-immunized mice.

Pulmonary cytokine responses of SARS-CoV-infected BALB/c mice previously immunized with recombinant VV expressing each structural protein of SARS-CoV

To elucidate the reason for the severe pulmonary inflammation observed in the mOrVV-NHis-immunized mice after SARS-CoV infection, we measured by quantitative RT-PCR the mRNA levels for various cytokines and chemokines in the lungs of BALB/c mice preimmunized with mOrVV-NHis, -MHis, -EHis, -SHis, or mO. Several proinflammatory cytokine and chemokine mRNAs, including those for IL-6, CXCL10, CCL2, and CCL3, were increased in all the groups, with the exception of the mOrVV-SHis group, 2 days after SARS-CoV infection (Fig. 6*A*). In contrast, the mOrVV-SHis-immunized group showed low levels of mRNA expression for these proinflammatory cytokines or chemokines, especially IL-6, resulting in reduced lung pathology after immunization. The mRNA levels for IFN-γ, IL-2, IL-4, and IL-5 were highest in the mOrVV-NHis-immunized group (Fig. 6, *A* and *B*). None of the other groups showed up-regulation of these cytokines, with the exception of the IL-5 mRNA level in the mOrVV-SHis-immunized group. Furthermore, the mRNA expression levels of anti-inflammatory cytokines (IL-10 and TGF-β) in the mOrVV-NHis-immunized group were markedly lower than expression levels in any of the other groups, which exhibited high virus titers, and were comparable to those of the mOrVV-SHis group, in which pulmonary inflammation was alleviated (Fig. 6*C*).

Verification of exacerbating effect of prior immunization with N protein in SARS-CoV-infected Balb/c mice

To verify the exacerbating effect of N protein immunization, we investigated the pulmonary virus titers and histopathology in BALB/c mice that were previously immunized with the combination of mOrVV-N and mOrVV-S (mOrVV-N+S-immunized group) 2 and 9 days after SARS-CoV infection, and compared them to those of all other groups, including the mO-, mOrVV-M+S-, mOrVV-E+S-, and mOrVV-S-immunized groups. The mOrVV-N+S-immunized group showed significantly decreased pulmonary virus titers compared with the mO-immunized group (Fig. 7*A*). However, the mOrVV-N+S-immunized group exhibited as

severe pneumonia as the mO-immunized group (Fig. 7, *B* and *C*). In contrast, both the mOrVV-M+S-immunized group and the mOrVV-E+S-immunized group were protected against SARS-CoV infection to the same extent as the mOrVV-S-immunized group (Fig. 7, *A–C*).

Discussion

SARS-CoV is newly identified as an agent of SARS. However, the detailed mechanism by which SARS-CoV causes severe pneumonia remains unclear. The uncontrolled release of immune mediators has been implicated in the pathogenesis of SARS, whereas the cytokine profiles of SARS patients have not elucidated the cause the pneumonia owing to their diversity. It seems likely that the diverse cytokine profiles noted among adult SARS patients are related to patient anamnesis.

In the present study, we observed severe pulmonary inflammation in m8rVV-NMES-immunized BALB/c mice 9 days after SARS-CoV infection (Fig. 4*A*, g), even though the initial virus titer was significantly lower than those of the control groups, which included vehicle- and m8-immunized mice (Fig. 3*B*). The severity of pulmonary inflammation did not correlate with the virus titer in the m8rVV-NMES-immunized mice, in contrast to the correlations observed for the vehicle-, m8-, and m8rVV-S-immunized groups. We identified the N protein of SARS-CoV as the cause of the severe pneumonia observed during SARS-CoV infection (Fig. 5, *C* and *D*, and 7, *B* and *C*). To date, no studies have been reported to our knowledge regarding SARS patients with severe pneumonia who were previously immunized with either SARS-CoV or a highly related species. In contrast, there are several reports of antisera against human CoV (229E and OC43) and host factor IL-11 cross-reacting with the SARS-CoV Ag (29, 30). Furthermore, the N protein of SARS-CoV has been shown to induce both cellular and humoral immune responses (31–33). Taken together, these results raise the possibility that a percentage of SARS patients already possess the adaptive immune response elements that can interact with SARS-CoV components, including the N protein, and that their adaptive immune response may be involved in the exacerbation of pneumonia. The temporal changes in immune response and the pathogenesis after SARS-CoV infection of an animal model that had previously been immunized with SARS-CoV components are not well understood, as almost all the previous studies reported only protection within a few days of SARS-CoV infection (34–39). In the present study, we demonstrate that mOrVV-NHis-immunized mice after SARS-CoV infection exhibit an imbalance between T cell activation (high expression levels of IFN-γ, IL-2, IL-4, and IL-5) and subsequent suppression (low expression levels of IL-10 and TGF-β), as well as high-level production of proinflammatory cytokines (IL-6 and TNF-α) and chemokines (CCL2, CCL3, and CXCL10). Jiang et al. (40) reported elevation of CXCL10 or IP-10 production in the pneumocytes, $CD3^+$ T cells, and monocytes and macrophages of the lungs of patients with SARS. CXCL10 may be responsible for the infiltration of activated T cells and monocytes or macrophages, which is a pathologic finding in SARS patients (41–43). It has been reported that elevated expression of monocyte or macrophage activation factors (CCL2 and CCL3) was observed in SARS patients (8, 44). Furthermore, the highest expression of IL-6 in mOrVV-NHis-immunized mice is reasonable (Fig. 6*A*), as the elevation of IL-6 levels is considered one of the causes in the severe pneumonia of SARS patients. Zhang et al. (45) reported recently the molecular mechanism of IL-6 expression induction by the N protein of SARS-CoV. In contrast, both IL-10 and TGF-β play important roles in suppressing inflammatory responses (46). Thus, the reduced production of both anti-inflammatory cytokines in the mOrVV-NHis-immunized mice after SARS-CoV infection may be related to the severity of the pulmonary inflammation in these mice. Weingartl et al. (47) and Czub et al. (48) reported that immunization with S protein expressing-recombinant modified VV Ankara (rMVA-S) induced stronger inflammatory responses and focal necrosis in liver tissues after SARS-CoV challenge than in control animals. However, the precise mechanism underlying this liver inflammation has not been clarified. Feline infectious peritonitis virus, which is another member of the coronavirus family, exhibits enhanced infection into monocytes or macrophages through virus-specific Ab binding to the Fc receptors of these cells and causes enhanced inflammation (49). It has also been reported for dengue virus that secondary infection with a different genotype results in more severe symptoms, including dengue hemorrhagic fever and dengue shock syndrome. The exacerbation of this symptom is also positively associated with pre-existing Abs with specificity for dengue virus (50). In the case of SARS-CoV, Ab-dependent enhancement of infection has not been reported previously. We hypothesized that the severe pneumonia observed in mOrVV-NHis-immunized mice after SARS-CoV infection does not result from Ab-dependent enhancement because the virus titers in the mouse lungs 9 days later were below the detection limit. Deming et al. (51) reported recently the intensive infiltration of eosinophils as well as lymphocytes after SARS-CoV infection of aged BALB/c mice previously immunized with the N protein of SARS-CoV. It has also been reported that immunization with formalin-inactivated respiratory syncytial virus vaccine and VV that expresses the G glycoprotein of respiratory syncytial virus correlates with the augmentation of Th2-type immune responses and enhanced pulmonary disease (52, 53). Therefore, the authors speculated that the Th2-biased responses of vaccinated hosts after SARS-CoV infection might aggravate pulmonary inflammation, although the main host response remains unknown. In contrast, our current data suggest that N protein-immunized mice exhibit activation of both Th1 and Th2 responses after SARS-CoV infection. In agreement with our data, Jin et al. (54) have demonstrated that prior immunization with N protein generates stronger Ag-specific Th1 and Th2 responses than immunization with M or E protein. In addition, we demonstrate the suppression of anti-inflammatory cytokine responses in N protein-immunized mice. Interestingly, Shi et al. (55) demonstrated that coinjection of M protein with N protein not only enhanced the production of Th1 cytokines (IFN-γ and IL-2), but also reduced the rates of mortality and pathologic change in SARS-CoV-infected voles. These results suggest that further studies, including epitope analysis, are required to reveal the precise mechanism underlying the severe pulmonary inflammation that results from SARS-CoV infection of BALB/c mice immunized with the N protein of SARS-CoV.

In contrast, intradermal immunization of aged BALB/c mice with m8rVV-S at 1×10^7 PFU/body significantly reduced the pulmonary virus titer 2 days after SARS-CoV infection (Fig. 3*B*). Furthermore, the m8rVV-S-immunized group exhibited alleviation of the pulmonary histopathology, as compared with both control groups after 9 days. To date, various types of SARS vaccine, including recombinant vaccines, inactivated vaccines, and DNA vaccine, have been reported (34–39). There are only a few reports on the effect of a single immunization with recombinant SARS vaccines, namely SARS-CoV S protein-expressing vaccines based on rabies virus (56), vesicular stomatitis virus (39), and adeno-associated virus (57). It is noteworthy that a single i.m. immunization with recombinant adeno-associated virus that expresses the receptor-binding domain of S protein conferred long-term protection against SARS-CoV infection (57). In the present study, we also show that a single immunization with m8rVV-S reduces viral load and improves the histopathologic findings in the lungs of BALB/c

mice infected with high-titer (1×10^5 $TCID_{50}$/body) SARS-CoV, although a relatively low titer of SARS-CoV was used in the previous study conducted by Du et al. (57). These results suggest that the systemic immune responses induced by a single immunization with SARS vaccine successfully protect the animal model against intranasal SARS-CoV infection.

In summary, we demonstrate that the immunization of BALB/c mice with the N protein of SARS-CoV causes severe pulmonary inflammation upon subsequent SARS-CoV infection, probably via the imbalance created between T cell activation and suppression, as well as by massive proinflammatory cytokine production. These results provide new insights into the mechanisms involved in the pathogenesis of SARS and help in the development of safe vaccines.

Acknowledgments

We are grateful to Dr. Ryuichi Miura (University of Tokyo) for arranging the SARS-CoV challenge experiment. We are also grateful to Iyo Kataoka (Institute of Medical Science, University of Tokyo). We thank Dr. Masahiro Shuda of the University of Pittsburgh for helpful discussions. We also thank Dr. Tetsuya Mizutani and Dr. Shigeru Morikawa (Department of Virology I, National Institute of Infectious Diseases) for providing antisera from rabbits immunized with the M protein peptide and inactivated SARS-CoV particles.

Disclosures

The authors have no financial conflict of interest.

References

1. Drosten, C., S. Gunther, W. Preiser, S. van der Werf, H. R. Brodt, S. Becker, H. Rabenau, M. Panning, L. Kolesnikova, R. A. Fouchier, et al. 2003. Identification of a novel coronavirus in patients with severe acute respiratory syndrome. *N. Engl. J. Med.* 348: 1967–1976.
2. Ksiazek, T. G., D. Erdman, C. S. Goldsmith, S. R. Zaki, T. Peret, S. Emery, S. Tong, C. Urbani, J. A. Comer, W. Lim, et al. 2003. A novel coronavirus associated with severe acute respiratory syndrome. *N. Engl. J. Med.* 1953–1966.
3. Peiris, J. S., S. T. Lai, L. L. Poon, Y. Guan, L. Y. Yam, W. Lim, J. Nicholls, W. K. Yee, W. W. Yan, M. T. Cheung, et al. 2003. Coronavirus as a possible cause of severe acute respiratory syndrome. *Lancet* 361: 1319–1325.
4. Rota, P. A., M. S. Oberste, S. S. Monroe, W. A. Nix, R. Campagnoli, J. P. Icenogle, S. Penaranda, B. Bankamp, K. Maher, M. H. Chen, et al. 2003. Characterization of a novel coronavirus associated with severe acute respiratory syndrome. *Science* 300: 1394–1399.
5. Li, W., M. J. Moore, N. Vasilieva, J. Sui, S. K. Wong, M. A. Berne, M. Somasundaran, J. L. Sullivan, K. Luzuriaga, T. C. Greenough, et al. 2003. Angiotensin-converting enzyme 2 is a functional receptor for the SARS coronavirus. *Nature* 426: 450–454.
6. Hamming, I., W. Timens, M. L. Bulthuis, A. T. Lely, G. J. Navis, and H. van Goor. 2004. Tissue distribution of ACE2 protein, the functional receptor for SARS coronavirus. A first step in understanding SARS pathogenesis. *J. Pathol.* 203: 631–637.
7. Jones, B. M., E. S. Ma, J. S. Peiris, P. C. Wong, J. C. Ho, B. Lam, K. N. Lai, and K. W. Tsang. 2004. Prolonged disturbances of in vitro cytokine production in patients with severe acute respiratory syndrome (SARS) treated with ribavirin and steroids. *Clin. Exp. Immunol.* 135: 467–473.
8. Wong, C. K., C. W. Lam, A. K. Wu, W. K. Ip, N. L. Lee, I. H. Chan, L. C. Lit, D. S. Hui, M. H. Chan, S. S. Chung, and J. J. Sung. 2004. Plasma inflammatory cytokines and chemokines in severe acute respiratory syndrome. *Clin. Exp. Immunol.* 136: 95–103.
9. Rowe, T., G. Gao, R. J. Hogan, R. G. Crystal, T. G. Voss, R. L. Grant, P. Bell, G. P. Kobinger, N. A. Wivel, and J. M. Wilson. 2004. Macaque model for severe acute respiratory syndrome. *J. Virol.* 78: 11401–11404.
10. Osterhaus, A. D., R. A. Fouchier, and T. Kuiken. 2004. The aetiology of SARS: Koch's postulates fulfilled. *Philos. Trans. R. Soc. Lond B Biol. Sci.* 359: 1081–1082.
11. Subbarao, K., J. McAuliffe, L. Vogel, G. Fahle, S. Fischer, K. Tatti, M. Packard, W. J. Shieh, S. Zaki, and B. Murphy. 2004. Prior infection and passive transfer of neutralizing antibody prevent replication of severe acute respiratory syndrome coronavirus in the respiratory tract of mice. *J. Virol.* 78: 3572–3577.
12. Glass, W. G., K. Subbarao, B. Murphy, and P. M. Murphy. 2004. Mechanisms of host defense following severe acute respiratory syndrome-coronavirus (SARS-CoV) pulmonary infection of mice. *J. Immunol.* 173: 4030–4039.
13. Roberts, A., L. Vogel, J. Guarner, N. Hayes, B. Murphy, S. Zaki, and K. Subbarao. 2005. Severe acute respiratory syndrome coronavirus infection of golden Syrian hamsters. *J. Virol.* 79: 503–511.
14. ter Meulen, J., A. B. Bakker, E. N. van den Brink, G. J. Weverling, B. E. Martina, B. L. Haagmans, T. Kuiken, J. de Kruif, W. Preiser, W. Spaan, et al. 2004. Human monoclonal antibody as prophylaxis for SARS coronavirus infection in ferrets. *Lancet* 363: 2139–2141.
15. Roberts, A., C. Paddock, L. Vogel, E. Butler, S. Zaki, and K. Subbarao. 2005. Aged BALB/c mice as a model for increased severity of severe acute respiratory syndrome in elderly humans. *J. Virol.* 79: 5833–5838.
16. Hong, T. C., Q. L. Mai, D. V. Cuong, M. Parida, H. Minekawa, T. Notomi, F. Hasebe, and K. Morita. 2004. Development and evaluation of a novel loop-mediated isothermal amplification method for rapid detection of severe acute respiratory syndrome coronavirus. *J. Clin. Microbiol.* 42: 1956–1961.
17. Kitabatake, M., S. Inoue, F. Yasui, S. Yokochi, M. Arai, K. Morita, H. Shida, M. Kidokoro, F. Murai, M. Q. Le, K. Mizuno, et al. 2007. SARS-CoV spike protein-expressing recombinant vaccinia virus efficiently induces neutralizing antibodies in rabbits pre-immunized with vaccinia virus. *Vaccine* 25: 630–637.
18. Hsieh, P. K., S. C. Chang, C. C. Huang, T. T. Lee, C. W. Hsiao, Y. H. Kou, I. Y. Chen, C. K. Chang, T. H. Huang, and M. F. Chang. 2005. Assembly of severe acute respiratory syndrome coronavirus RNA packaging signal into virus-like particles is nucleocapsid dependent. *J. Virol.* 79: 13848–13855.
19. Zhang, C. H., J. H. Lu, Y. F. Wang, H. Y. Zheng, S. Xiong, M. Y. Zhang, X. J. Liu, J. X. Li, Z. Y. Wan, X. G. Yan, et al. 2005. Immune responses in BALB/c mice induced by a candidate SARS-CoV inactivated vaccine prepared from F69 strain. *Vaccine* 23: 3196–3201.
20. Biacchesi, S., M. H. Skiadopoulos, L. Yang, B. R. Murphy, P. L. Collins, and U. J. Buchholz. 2005. Rapid human metapneumovirus microneutralization assay based on green fluorescent protein expression. *J. Virol. Methods* 128: 192–197.
21. Cimolai, N., G. P. Taylor, D. Mah, and B. J. Morrison. 1992. Definition and application of a histopathological scoring scheme for an animal model of acute *Mycoplasma pneumoniae* pulmonary infection. *Microbiol. Immunol.* 36: 465–478.
22. Luna, L. G., 1968. *Manual of Histologic Staining Methods of the Armed Forces Institute of Pathology*. McGraw-Hill, New York, p. 111.
23. Voss, D., A. Kern, E. Traggiai, M. Eickmann, K. Stadler, A. Lanzavecchia, and S. Becker. 2006. Characterization of severe acute respiratory syndrome coronavirus membrane protein. *FEBS Lett.* 580: 968–973.
24. Ho, Y., P. H. Lin, C. Y. Liu, S. P. Lee, and Y. C. Chao. 2004. Assembly of human severe acute respiratory syndrome coronavirus-like particles. *Biochem. Biophys. Res. Commun.* 318: 833–838.
25. Huang, Y., Z. Y. Yang, W. P. Kong, and G. J. Nabel. 2004. Generation of synthetic severe acute respiratory syndrome coronavirus pseudoparticles: implications for assembly and vaccine production. *J. Virol.* 78: 12557–12565.
26. Buchholz, U. J., A. Bukreyev, L. Yang, E. W. Lamirande, B. R. Murphy, K. Subbarao, and P. L. Collins. 2004. Contributions of the structural proteins of severe acute respiratory syndrome coronavirus to protective immunity. *Proc. Natl. Acad. Sci. USA* 101: 9804–9809.
27. Kim, T. W., J. H. Lee, C. F. Hung, S. Peng, R. Roden, M. C. Wang, R. Viscidi, Y. C. Tsai, L. He, P. J. Chen, et al. 2004. Generation and characterization of DNA vaccines targeting the nucleocapsid protein of severe acute respiratory syndrome coronavirus. *J. Virol.* 78: 4638–4645.
28. Fan, B. X., L. X. Xie, L. A. Chen, W. J. Chen, J. Wen, and Y. N. Liu. 2005. Study on the dynamics of IgG antibody in 311 patients with severe acute respiratory syndrome. *Zhonghua Liu Xing Bing Xue Za Zhi.* 26: 194–196.
29. Che, X. Y., L. W. Qiu, Z. Y. Liao, Y. D. Wang, K. Wen, Y. X. Pan, W. Hao, Y. B. Mei, V. C. Cheng, and K. Y. Yuen. 2005. Antigenic cross-reactivity between severe acute respiratory syndrome-associated coronavirus and human coronaviruses 229E and OC43. *J. Infect. Dis.* 191: 2033–2037.
30. Cheng, M., C. W. Chan, R. C. Cheung, R. K. Bikkavilli, Q. Zhao, S. W. Au, P. K. Chan, S. S. Lee, G. Cheng, W. K. Ho, and W. T. Cheung. 2005. Cross-reactivity of antibody against SARS-coronavirus nucleocapsid protein with IL-11. *Biochem. Biophys. Res. Commun.* 338: 1654–1660.
31. Liu, S. J., C. H. Leng, S. P. Lien, H. Y. Chi, C. Y. Huang, C. L. Lin, W. C. Lian, C. J. Chen, S. L. Hsieh, and P. Chong. 2006. Immunological characterizations of the nucleocapsid protein based SARS vaccine candidates. *Vaccine* 24: 3100–3108.
32. Zhu, M. S., Y. Pan, H. Q. Chen, Y. Shen, X. C. Wang, Y. J. Sun, and K. H. Tao. 2004. Induction of SARS-nucleoprotein-specific immune response by use of DNA vaccine. *Immunol. Lett.* 92: 237–243.
33. Zhao, J., Q. Huang, W. Wang, Y. Zhang, P. Lv, and X. M. Gao. 2007. Identification and characterization of dominant helper T-cell epitopes in the nucleocapsid protein of severe acute respiratory syndrome coronavirus. *J. Virol.* 81: 6079–6088.
34. Yang, Z. Y., W. P. Kong, Y. Huang, A. Roberts, B. R. Murphy, K. Subbarao, and G. J. Nabel. 2004. A DNA vaccine induces SARS coronavirus neutralization and protective immunity in mice. *Nature* 428: 561–564.
35. Bukreyev, A., E. W. Lamirande, U. J. Buchholz, L. N. Vogel, W. R. Elkins, M. St Claire, B. R. Murphy, K. Subbarao, and P. L. Collins. 2004. Mucosal immunisation of African green monkeys (*Cercopithecus aethiops*) with an attenuated parainfluenza virus expressing the SARS coronavirus spike protein for the prevention of SARS. *Lancet* 363: 2122–2127.
36. Zhi, Y., J. Figueredo, G. P. Kobinger, H. Hagan, R. Calcedo, J. R. Miller, G. Gao, and J. M. Wilson. 2006. Efficacy of severe acute respiratory syndrome vaccine based on a nonhuman primate adenovirus in the presence of immunity against human adenovirus. *Hum. Gene Ther.* 17: 500–506.
37. Bisht, H., A. Roberts, L. Vogel, K. Subbarao, and B. Moss. 2005. Neutralizing antibody and protective immunity to SARS coronavirus infection of mice induced by a soluble recombinant polypeptide containing an N-terminal segment of the spike glycoprotein. *Virology* 334: 160–165.
38. Bisht, H., A. Roberts, L. Vogel, A. Bukreyev, P. L. Collins, B. R. Murphy, K. Subbarao, and B. Moss. 2004. Severe acute respiratory syndrome coronavirus

spike protein expressed by attenuated vaccinia virus protectively immunizes mice. *Proc. Natl. Acad. Sci. USA* 101: 6641–6646.
39. Kapadia, S. U., J. K. Rose, E. Lamirande, L. Vogel, K. Subbarao, and A. Roberts. 2005. Long-term protection from SARS coronavirus infection conferred by a single immunization with an attenuated VSV-based vaccine. *Virology* 340: 174–182.
40. Jiang, Y., J. Xu, C. Zhou, Z. Wu, S. Zhong, J. Liu, W. Luo, T. Chen, Q. Qin, and P. Deng. 2005. Characterization of cytokine/chemokine profiles of severe acute respiratory syndrome. *Am. J. Respir. Crit. Care Med.* 171: 850–857.
41. Franks, T. J., P. Y. Chong, P. Chui, J. R. Galvin, R. M. Lourens, A. H. Reid, E. Selbs, C. P. McEvoy, C. D. Hayden, J. Fukuoka, et al. 2003. Lung pathology of severe acute respiratory syndrome (SARS): a study of 8 autopsy cases from Singapore. *Hum. Pathol.* 34: 743–748.
42. Nicholls, J. M., L. L. Poon, K. C. Lee, W. F. Ng, S. T. Lai, C. Y. Leung, C. M. Chu, P. K. Hui, K. L. Mak, W. Lim, et al. 2003. Lung pathology of fatal severe acute respiratory syndrome. *Lancet* 361: 1773–1778.
43. Ding, Y., H. Wang, H. Shen, Z. Li, J. Geng, H. Han, J. Cai, X. Li, W. Kang, D. Weng, et al. 2003. The clinical pathology of severe acute respiratory syndrome (SARS): a report from China. *J. Pathol.* 200: 282–289.
44. He, L., Y. Ding, Q. Zhang, X. Che, Y. He, H. Shen, H. Wang, Z. Li, L. Zhao, J. Geng, et al. 2006. Expression of elevated levels of pro-inflammatory cytokines in SARS-CoV-infected ACE2+ cells in SARS patients: relation to the acute lung injury and pathogenesis of SARS. *J. Pathol.* 210: 288–297.
45. Zhang, X., K. Wu, D. Wang, X. Yue, D. Song, Y. Zhu, and J. Wu. 2007. Nucleocapsid protein of SARS-CoV activates interleukin-6 expression through cellular transcription factor NF-κB. *Virology* 365: 324–335.
46. Fuss, I. J., M. Boirivant, B. Lacy, and W. Strober. 2002. The interrelated roles of TGF-β and IL-10 in the regulation of experimental colitis. *J. Immunol.* 168: 900–908.
47. Weingartl, H., M. Czub, S. Czub, J. Neufeld, P. Marszal, J. Gren, G. Smith, S. Jones, R. Proulx, Y. Deschambault, et al. 2004. Immunization with modified vaccinia virus Ankara-based recombinant vaccine against severe acute respiratory syndrome is associated with enhanced hepatitis in ferrets. *J. Virol.* 78: 12672–12676.
48. Czub, M., H. Weingartl, S. Czub, R. He, and J. Cao. 2005. Evaluation of modified vaccinia virus Ankara based recombinant SARS vaccine in ferrets. *Vaccine* 23: 2273–2279.
49. Corapi, W. V., C. W. Olsen, and F. W. Scott. 1992. Monoclonal antibody analysis of neutralization and antibody-dependent enhancement of feline infectious peritonitis virus. *J. Virol.* 66: 6695–6705.
50. Halstead, S. B. 1982. Immune enhancement of viral infection. *Prog. Allergy* 31: 301–364.
51. Deming, D., T. Sheahan, M. Heise, B. Yount, N. Davis, A. Sims, M. Suthar, J. Harkema, A. Whitmore, R. Pickles, et al. 2006. Vaccine efficacy in senescent mice challenged with recombinant SARS-CoV bearing epidemic and zoonotic spike variants. *PLoS Med.* 3:e525.
52. Boelen, A., A. Andeweg, J. Kwakkel, W. Lokhorst, T. Bestebroer, J. Dormans, and T. Kimman. 2000. Both immunisation with a formalin-inactivated respiratory syncytial virus (RSV) vaccine and a mock antigen vaccine induce severe lung pathology and a Th2 cytokine profile in RSV-challenged mice. *Vaccine* 19: 982–991.
53. Johnson, T. R., J. E. Johnson, S. R. Roberts, G. W. Wertz, R. A. Parker, and B. S. Graham. 1998. Priming with secreted glycoprotein G of respiratory syncytial virus (RSV) augments interleukin-5 production and tissue eosinophilia after RSV challenge. *J. Virol.* 72: 2871–2880.
54. Jin, H., C. Xiao, Z. Chen, Y. Kang, Y. Ma, K. Zhu, Q. Xie, Y. Tu, Y. Yu, and B. Wang. 2005. Induction of Th1 type response by DNA vaccinations with N, M, and E genes against SARS-CoV in mice. *Biochem. Bbiophys. Res. Commun.* 328: 979–986.
55. Shi, S. Q., J. P. Peng, Y. C. Li, C. Qin, G. D. Liang, L. Xu, Y. Yang, J. L. Wang, and Q. H. Sun. 2006. The expression of membrane protein augments the specific responses induced by SARS-CoV nucleocapsid DNA immunization. *Mol. Immunol.* 43: 1791–1798.
56. Faber, M., E. W. Lamirande, A. Roberts, A. B. Rice, H. Koprowski, B. Dietzschold, and M. J. Schnell. 2005. A single immunization with a rhabdovirus-based vector expressing severe acute respiratory syndrome coronavirus (SARS-CoV) S protein results in the production of high levels of SARS-CoV-neutralizing antibodies. *J. Gen. Virol.* 86: 1435–1440.
57. Du, L., G. Zhao, Y. Lin, H. Sui, C. Chan, S. Ma, Y. He, S. Jiang, C. Wu, K. Y. Yuen, et al. 2008. Intranasal vaccination of recombinant adeno-associated virus encoding receptor-binding domain of severe acute respiratory syndrome coronavirus (SARS-CoV) spike protein induces strong mucosal immune responses and provides long-term protection against SARS-CoV infection. *J. Immunol.* 180: 948–956.

doi:10.1111/j.1440-1746.2007.05076.x

HEPATOLOGY

Inhibition of hepatitis C virus infection and expression *in vitro* and *in vivo* by recombinant adenovirus expressing short hairpin RNA

Naoya Sakamoto,*,† Yoko Tanabe,* Takanori Yokota,‡ Kenichi Satoh,§ Yuko Sekine-Osajima,* Mina Nakagawa,*,† Yasuhiro Itsui,* Megumi Tasaka,* Yuki Sakurai,* Chen Cheng-Hsin,* Masahiko Yano,¶ Shogo Ohkoshi,¶ Yutaka Aoyagi,¶ Shinya Maekawa,†† Nobuyuki Enomoto,†† Michinori Kohara§ and Mamoru Watanabe*

Departments of *Gastroenterology and Hepatology, †Hepatitis Control, and ‡Neurology and Neurological Science, Tokyo Medical and Dental University, §Department of Microbiology and Cell Biology, The Tokyo Metropolitan Institute of Medical Science, Tokyo, ¶Gastroenterology and Hepatology Division, Graduate School of Medical and Dental Sciences, Niigata University, Niigata, and ††First Department of Medicine, Yamanashi University, Yamanashi, Japan

Key words
adenovirus vector, hepatitis C virus, RNA interference.

Accepted for publication 12 April 2007.

Correspondence
Dr Naoya Sakamoto, Department of Gastroenterology and Hepatology, Tokyo Medical and Dental University, 1-5-45 Yushima, Bunkyo-ku, Tokyo 113-8519, Japan.
Email: nsakamoto.gast@tmd.ac.jp

NS and YT have contributed equally to this paper.

Abstract

Background and Aim: We have reported previously that synthetic small interfering RNA (siRNA) and DNA-based siRNA expression vectors efficiently and specifically suppress hepatitis C virus (HCV) replication *in vitro*. In this study, we investigated the effects of the siRNA targeting HCV-RNA *in vivo*.

Methods: We constructed recombinant retrovirus and adenovirus expressing short hairpin RNA (shRNA), and transfected into replicon-expressing cells *in vitro* and transgenic mice *in vivo*.

Results: Retroviral transduction of Huh7 cells to express shRNA and subsequent transfection of an HCV replicon into the cells showed that the cells had acquired resistance to HCV replication. Infection of cells expressing the HCV replicon with an adenovirus expressing shRNA resulted in efficient vector delivery and expression of shRNA, leading to suppression of the replicon in the cells by $\sim 10^{-5}$. Intravenous delivery of the adenovirus expressing shRNA into transgenic mice that can be induced to express HCV structural proteins by the Cre/*lox*P switching system resulted in specific suppression of virus protein synthesis in the liver.

Conclusion: Taken together, our results support the feasibility of utilizing gene targeting therapy based on siRNA and/or shRNA expression to counteract HCV replication, which might prove valuable in the treatment of hepatitis C.

Introduction

Hepatitis C virus (HCV), which affects 170 million people worldwide, is one of the most important pathogens causing liver-related morbidity and mortality.[1] The difficulty in eradicating HCV is attributable to limited treatment options against the virus and their unsatisfactory efficacies. Even with the most effective regimen with pegylated interferon (IFN) and ribavirin in combination, the efficacies are limited to less than half of the patients treated.[2] Given this situation, the development of safe and effective anti-HCV therapies is one of our high-priority goals.

RNA interference (RNAi) is a process of sequence-specific, post-transcriptional gene silencing that is initiated by double-stranded RNA.[3,4] Because of its potency and specificity, RNAi rapidly has become a powerful tool for basic research to analyze gene functions and for potential therapeutic applications. Recently, successful suppression of various human pathogens by RNAi have been reported, including human immunodeficiency viruses,[5,6] poliovirus,[7] influenza virus,[8] severe acute respiratory syndrome (SARS) virus[9] and hepatitis B virus (HBV).[10–13]

We and other researchers have reported that appropriately designed small interfering RNA (siRNA) targeting HCV genomic RNA can efficiently and specifically suppress HCV replication *in vitro*.[14–19] We have tested siRNA designed to target the well-conserved 5′-untranslated region (5′-UTR) of HCV-RNA, and identified the most effective target, just upstream of the translation initiation codon. Furthermore, transfection of DNA-based vectors expressing siRNA was as effective as that of synthetic siRNA in suppressing HCV replication.[14]

In this study, we explored the further possibility that efficient delivery and expression of siRNA may be effective in suppression and elimination of HCV replication and that delivery of such

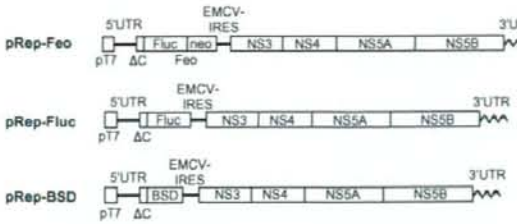

Figure 1 Structures of HCV replicon plasmids. The pRep-Feo expressed a chimeric reporter protein of firefly luciferase (Fluc) and neomycin phosphotransferase (GenBank accession No. AB119282).[14,20] The pRep-Fluc expressed the Fluc protein. The pRep-BSD expressed the blasticidin S (BSD) resistance gene. pT7, T7 promoter; 5'UTR, HCV 5'-untranslated region; ΔC, truncated HCV core region (nt. 342–377); neo, neomycin phosphotransferase gene; EMCV, encephalomyocarditis virus; NS3, NS4, NS5A and NS5B, genes that encode HCV non-structural proteins; 3'UTR, HCV 3'-untranslated region.

HCV-directed siRNA *in vivo* may be effective in silencing viral protein expression in the liver. Here, we report that HCV replication was suppressed *in vitro* by recombinant retrovirus and adenovirus vectors expressing short hairpin RNA (shRNA) and that the delivery of the adenovirus vector to mice *in vivo* specifically inhibited viral protein synthesis in the liver.

Methods

Cells and cell culture

Huh7 and Retro Pack PT67 cells (Clontech, Palo Alto, CA, USA) were maintained in Dulbecco's modified minimal essential medium (Sigma, St. Louis, MO, USA) supplemented with 10% fetal calf serum at 37°C under 5% CO_2. To maintain cell lines carrying the HCV replicon, G418 (Wako, Osaka, Japan) was added to the culture medium to a final concentration of 500 μg/mL.

HCV replicon constructs and transfection

HCV replicon plasmids, pRep-Feo, pRep-Fluc and pRep-BSD were constructed from were constructed from a virus, HCV-N strain, genotype 1b.[21] The pRep-Feo expressed a chimeric reporter protein of firefly luciferase (Fluc) and neomycin phosphotransferase.[14,20] The pRep-Fluc and the pRep-BSD expressed the Fluc and blasticidin S (BSD) resistance genes, respectively (Fig. 1). The replicon RNA synthesis and the transfection protocol have been described previously.[22]

Synthetic siRNA and siRNA-expression plasmid

The design and construction of HCV-directed siRNA vectors have been described.[14] Briefly, five siRNA targeting the 5'-UTR of HCV RNA were tested for their efficiency to inhibit HCV replication, and the most effective sequence, which targeted nucleotide position of 331 though 351, was used in the present study. To construct shRNA-expressing DNA cassettes, oligonucleotide inserts were synthesized that contained the loop sequence (5'-TTC AAG AGA-3') flanked by sense and antisense siRNA sequences (Fig. 2a). These were inserted immediately downstream of the human U6 promoter. To avoid a problem in transcribing shRNA because of instability of the DNA strands arising from the tight palindrome structure, several C-to-T point mutations, which retained completely the silencing activity of the shRNA, were introduced into the sense strand of the shRNA sequences (referred to as 'm').[23] A control plasmid, pUC19-shRNA-Control, expressed shRNA directed towards the Machado–Joseph disease gene, which is a mutant of ataxin-3 gene and is not normally expressed. We have previously described the sequence specific activity of the shRNA-Control.[24]

Prior to construction of the virus vectors, we tested silencing efficiency of five shRNA constructs of different lengths that covered the target sequence (Fig. 2a). The shRNA-HCV-19, shRNA-HCV-21 and shRNA-HCV-27 had target sequences of 19, 21 and 27 nucleotides, respectively. Transfection of these shRNA constructs into Huh7/pRep-Feo showed that shRNA with longer target sequences had better suppressive effects (Fig. 2b). Therefore, we used shRNA-HCV-27m (abbreviated as shRNA-HCV) in the following study.

Recombinant retrovirus vectors

The U6-shRNA expression cassettes were inserted into the *StuI*/*Hin*dIII site of a retrovirus vector, pLNCX2 (Clontech) to construct pLNCshRNA-HCV and pLNCshRNA-Control (Fig. 2c). The plasmids were transfected into the packaging cells, Retro Pack PT67. The culture supernatant was filtered and added onto Huh7 cells with 4 μg/mL of polybrene. Huh7 cell lines stably expressing shRNA were established by culture in the presence of 500 μg/mL of G418.

Recombinant adenovirus

Recombinant adenoviruses expressing shRNA were constructed using an Adenovirus Expression Vector Kit (Takara, Otsu, Japan). The U6-shRNA expression DNA cassette was inserted into the *SwaI* site of pAxcw to construct pAxshRNA-HCV and pAxshRNA-Control. The adenoviruses were propagated according to the manufacturer's protocol (AxshRNA-HCV and AxshRNA-Control; Fig. 2c). A 'multiplicity of infection' (MOI) was used to standardize infecting doses of adenovirus. The MOI stands for the ratio of infectious virus particles to the number of cells being infected. An MOI = 1 represents equivalent dose to introduce one infectious virus particle to every host cell that is present in the culture.

Plasmids for assays of interferon responses

pISRE-TA-Luc (Invitrogen, Carlsbad, CA, USA) contained five copies of the consensus interferon stimulated response element (ISRE) motifs upstream of the Fluc gene. pTA-Luc (Invitrogen), which lacks the enhancer element, was used for background determination. The pcDNA3.1 (Invitrogen) was used as an empty vector for mock transfection. pRL-CMV (Promega, Madison, WI, USA), which expresses the *Renilla* luciferase protein, was used for normalization of transfection efficiency.[25] A plasmid, peGFPneo (Invitrogen), was used to monitor percentages of transduced cells.

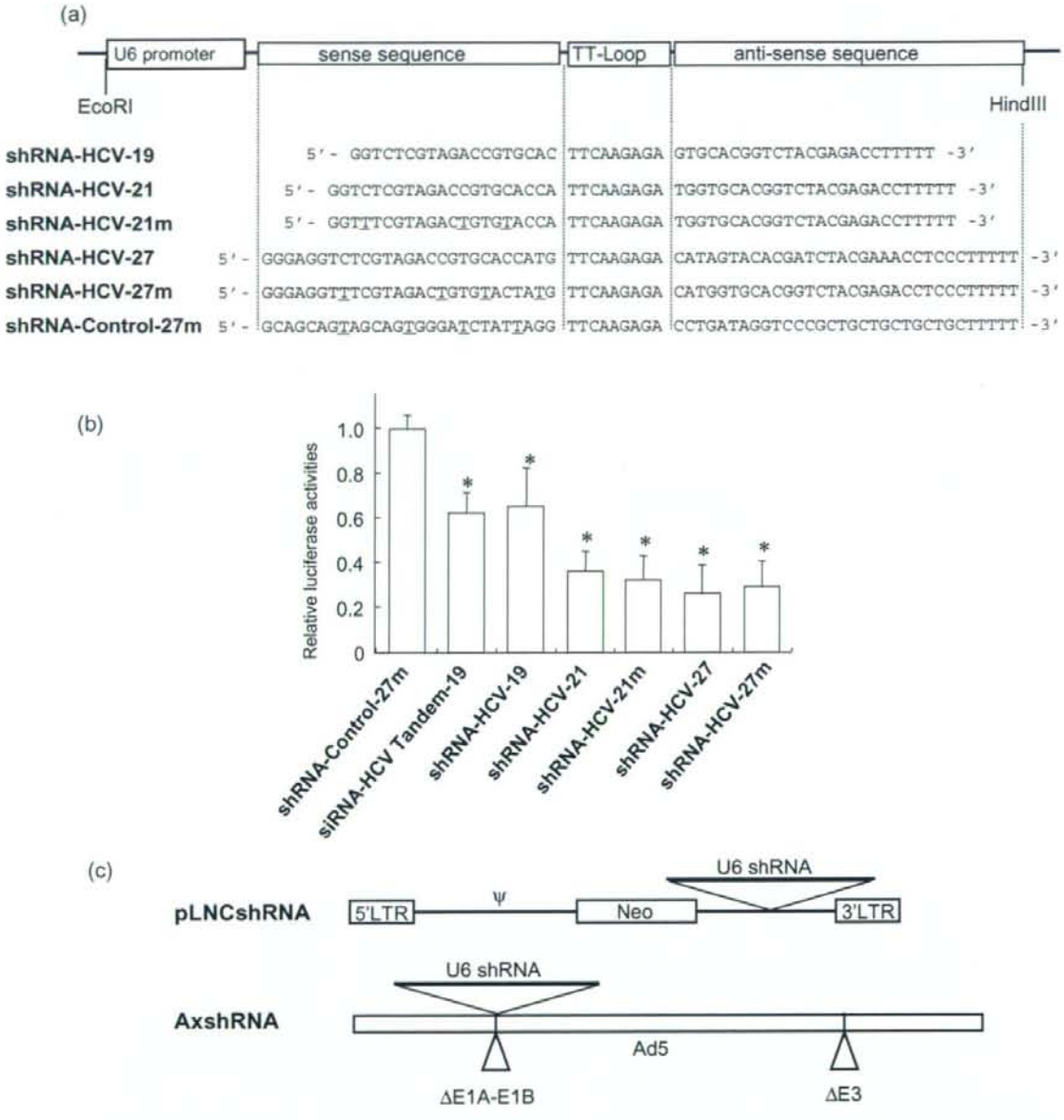

Figure 2 Structure of shRNA-expression constructs and shRNA sequences. (a) Structure of shRNA-expression cassette and shRNA sequences. TT-Loop, the loop sequence. The shRNA-Control was directed toward an unrelated target, Machado–Joseph disease gene. Underlined letters indicate C-to-T point mutations in the sense strand. (b) The shRNA-expression plasmids were transfected into Huh7/pRep-Feo cells, and internal luciferase activities were measured at 48 h of transfection. Each assay was done in triplicate, and the values are displayed as mean + SD. $^*P < 0.05$. (c) pLNCshRNA, structure of a recombinant retrovirus expressing shRNA. Ψ, the retroviral packaging signal sequence. AxshRNA, structure of a recombinant adenovirus expressing shRNA.